

Coevolution (Or Not) of Supermassive Black Holes and Host Galaxies

John Kormendy¹ and Luis C. Ho^{2,3}

¹Department of Astronomy, University of Texas at Austin,
2515 Speedway C1400, Austin, TX 78712-1205; email: kormendy@astro.as.utexas.edu

²The Observatories of the Carnegie Institution for Science,
813 Santa Barbara Street, Pasadena, CA 91101; email: lho@obs.carnegiescience.edu

³Kavli Institute for Astronomy and Astrophysics,
Peking University, Beijing 100871, China (Starting 2014 January)

SUPPLEMENTAL MATERIAL

Section S1 is a supplement to main paper Section 3 on machinery to measure BH masses M_{\bullet} . It summarizes indirect methods that are used to estimate M_{\bullet} in AGNs. These are used sparingly in main paper Section 6.9, Sections 7.1–7.3, Sections 8.3, 8.5, and 8.6, and Section 9.

Section S2 lists the observational criteria that we use to classify classical and pseudo bulges. Section 4 in the main paper introduces the physical distinction between remnants of major mergers and pseudo (“fake”) bulges that were grown slowly out of disks, not made rapidly in violent events. This distinction is central to Sections 5–9. However, the (pseudo)bulge classifications used in this paper are not based on interpretation; they are based on the Section S2 observational criteria.

Section S3 supplements the BH database in Section 5 of the main paper and Section S4 here. It discusses corrections to galaxy and BH parameters, most importantly to 2MASS K -band apparent magnitudes. They are needed because 2MASS misses light at large radii when the images of galaxies subtend large angles on the sky or have shallow outer brightness gradients. These corrections are included in **Tables 2** and **3**, which are numbered consistently here and in the main paper.

Section S4 reproduces essentially verbatim the first part of Section 5 in the main paper, the BH database, including the list of BH and host-galaxy properties (**Tables 2** and **3**). Its purpose is to provide notes on the properties given in the tables, especially all of the notes on individual objects. To save space, only a few examples of these notes are included in the main paper.

S1. BH MASS MEASUREMENTS FOR ACTIVE GALAXIES

The methods reviewed in Sections 3.1–3.3 provide the most direct BH masses (**Tables 2** and **3**) and lead to most of the demographic results discussed in this paper. But these methods have two limitations. It is difficult to study late-type galaxies, starbursting galaxies, and AGNs. This makes it harder to connect BH demographics with theories of galaxy formation. And these methods require us to spatially resolve the sphere-of-influence radius r_{infl} of the BH. Success is limited to nearby galaxies. Most AGNs are so distant that we cannot resolve r_{infl} . In any case, the bright glare from the active nucleus often overwhelms the stellar features in host-galaxy spectra. Also, the kinematics of circumnuclear ionized gas can easily be perturbed by non-gravitational forces such as radiation pressure or shocks. The unfortunate consequence is that the objects whose current activity most directly tells us about BH-host coevolution are excluded from direct dynamical study.

Much work has gone into using AGNs to solve these problems. This section summarizes the machinery used to estimate BH masses in AGNs. We cover only the bare essentials and do not attempt a comprehensive review of this extensive subject. Recent reviews can be found in Peterson (2011) and Shen (2013).

S1.1. Reverberation Mapping

This technique is based on the assumption that the broad emission lines observed in the UV and optical spectra of quasars and Seyfert 1 galaxies come from gravity-dominated regions close to the BH. If the velocity widths of the emission lines trace the virial velocity ΔV of the broad-line region (BLR) at radius r , then

$$M_{\bullet} = \frac{f(\Delta V)^2 r}{G}. \quad (\text{S1})$$

Most of our astrophysical ignorance is lumped into the factor f , which depends on the geometry and detailed kinematics of the BLR.

BLRs have radii of a few light days to a few light weeks, so we cannot resolve them spatially. However, we can resolve them temporally using a technique known as reverberation mapping (Blandford & McKee 1982). Its origins trace back to Bahcall, Kozlovsky, & Salpeter (1972), Lyutyi & Cherepashchuk (1972), and Cherepashchuk & Lyutyi (1973). The physical basis is simple. The broad emission lines arise from clouds that are photoionized by the UV radiation from the hot, inner parts of the accretion disk. When this ionizing continuum varies in brightness, the broad emission lines vary (“reverberate”) in response, but their brightness variations are delayed by a time lag $\tau = r/c$ equal to the light travel time between the continuum source and the location of the line-emitting gas. To date, reverberation mapping experiments have yielded line-continuum lag measurements for approximately 50 type 1 AGNs (Kaspi et al. 2000; Peterson et al. 2004; Bentz et al. 2008, 2009b; Denney et al. 2010; Barth et al. 2011; Grier et al. 2012). Most observations concentrate on H β (and to a lesser extent H α); much less data exist for Mg II or C IV. The current sample is strongly biased toward relatively low-luminosity AGNs, mostly nearby Seyfert 1 galaxies. A number of Palomar-Green (Schmidt & Green 1983) quasars are included, but the highest-redshift source studied is only at $z = 0.29$ (PG 1700+518). This reflects the historical roots of how samples were assembled and the practical challenges of spectroscopically monitoring higher- z quasars (Kaspi et al. 2007; Trevese et al. 2007; Woo 2008).

The resulting BLR sizes can be combined with velocity width measures to calculate M_{\bullet} . However, implementing Equation S1 involves a practical problem. What part of the emission-line profile should we use? And how does it measure the virial velocity ΔV ? Popular choices are $\Delta V = \text{FWHM}$ and $\Delta V = \sigma_{\text{line}}$, i. e., the second moment of the line profile. Opinions vary as to which ΔV indicator is better (e. g., Peterson et al. 2004; Collin et al. 2006; see Shen 2013 for a review). By far the biggest uncertainty is the virial coefficient f . It is unknown, and it probably varies from source to source. A spherical distribution of clouds on random, isotropic orbits has $f = 3/4$ for $\Delta V = \text{FWHM}$ and $f = 3$ for $\Delta V = \sigma_{\text{line}}$ (Netzer 1990). However, this idealization is almost certainly too simplistic. In principle, f can be constrained using sufficiently accurate velocity-resolved delay maps (e. g., Denney et al. 2009; Bentz et al. 2010; Grier et al. 2013), but such measurements are still rare and uncertain. Direct dynamical modeling may eventually bypass the need to adopt an f factor (Brewer et al. 2011; Pancoast et al. 2011, 2012). For the time being, a practical way forward is to calibrate an average value of f for the sample of reverberation-mapped objects by requiring that they follow the same $M_{\bullet} - \sigma$ relation as inactive galaxies. This is a reasonable but unproven assumption. It is motivated by the empirical fact that reverberation-mapped AGNs—at least those that have bulge stellar velocity dispersion measurements—do seem to follow an $M_{\bullet} - \sigma$ relation (Gebhardt et al. 2000a; Ferrarese et al. 2001; Nelson et al. 2004; Greene & Ho 2006). Following this approach and adopting the $M_{\bullet} - \sigma$ relation of Tremaine et al. (2002) as the fiducial reference, Onken et al. (2004) used 14 reverberation-mapped AGNs to obtain $\langle f \rangle = 5.5 \pm 1.8$ for $\Delta V = \sigma_{\text{line}}$. The scatter in M_{\bullet} for AGNs is surprisingly small, less than a factor of 3. Woo et al. (2010) enlarged the calibration sample to 24 objects and found $\langle f \rangle = 5.2 \pm 1.2$ with respect to the $M_{\bullet} - \sigma$ relation of Gültekin et al. (2009c) and an intrinsic scatter of 0.44 ± 0.07 dex. Park et al. (2012) discuss uncertainties resulting from different fitting methods and the use of different reference samples of inactive galaxies.

Equation S1 depends on the assumption that BLR velocities are controlled by BH gravity. (Other caveats are discussed in Krolik 2001 and in Greene & Ho 2009.) Outflows at velocities that are

FWHM: Full width of the line profile at half of maximum intensity

much larger than the escape velocity would cause us to overestimate M_{\bullet} . Gas responds easily to non-gravitational forces. An AGN is intrinsically a high-radiation-flux environment. Winds and outflows are pervasive. Successful tests that BLR gas clouds move at velocities that are comparable to those in virial equilibrium are therefore central to our confidence in using this methodology.

Velocity-resolved reverberation mapping provides this test. The early study by Gaskell (1988) established the principle. If gas flows outward, then the near side of the BLR moves toward us and the far side moves away from us. Therefore, the blue wings of the emission lines should vary first and the red wings should vary $\Delta\tau \simeq 2r \tan i/c$ later. Infall results in the opposite behavior. From the emission lines C IV λ 1549 and Mg II λ 2798, Gaskell (1988) found that outflow is excluded in NGC 4151. Shorter lags for the red wings were most consistent with infall, although circular + random motions were not strongly excluded. The conclusion was that gravity controls the motions and that $M_{\bullet} \sim (5 \text{ to } 10) \times 10^7 M_{\odot}$. Koratkar & Gaskell (1989) got similar results for Fairall 9. Gaskell (2010) reviews additional tests. The cleanest infall signature is seen in Arp 151, observed as part of the Lick AGN Monitoring Project (LAMP: Bentz et al. 2008, 2009b, 2010). Most reverberation observations are consistent with virialized motions or with some infall (Bentz et al. 2010). A few exceptions (e. g., Denney et al. 2009) emphasize the need for long or repeated observing campaigns. Note that free fall from infinity in an M_{\bullet} -dominated potential results in a radial $V \propto 1/\sqrt{r}$ velocity field. If AGNs have a distribution of small infall velocities in addition to mainly circular or random virial cloud motions, this infall will be “calibrated out” in the determination of the factor f .

A critical consistency check is that different reverberation lags for different emission lines in the same object should give the same M_{\bullet} . BLR emission lines have different excitation potentials and so are emitted at different temperatures and radii. If line widths measure Keplerian velocities, then different line widths at different radii should anticorrelate with lag τ as $\Delta V \propto 1/\sqrt{c\tau}$. The best-observed galaxy, NGC 5548, shows this correlation convincingly, as do three other sources (Peterson 2011). Recently, LAMP has substantially “raised the bar” on reverberation mapping and extended this test successfully to many more objects (Bentz et al. 2010).

On the other hand, a concern is raised by the observation that the BLR structure changes with emission-line FWHM (Kollatschny & Zetzl 2011). They show that $\text{FWHM}/\sigma_{\text{line}}$ is a strong, smooth function of FWHM, ranging from 0.5 at $\text{FWHM} \simeq 1000 \text{ km s}^{-1}$ to 3 at $\text{FWHM} \simeq 12000 \text{ km s}^{-1}$. These changes in line profile shapes suggest that the balance between rotation, random velocities, and in- or outflow changes with line width. Hints of this were seen in earlier work (Collin et al. 2006; Marziani & Sulentic 2012). Implications are worrisome: f must depend on FWHM and σ_{line} .

Another fundamental limitation is implied by the conclusion (Gaskell 2008, 2011) that AGN continua can flare in localized, off-center patches not far inside the BLR radius. This produces noise. Clearly M_{\bullet} should be based on as many lines and as many observing campaigns as possible.

*We emphasize an important shortcoming in all calibrations of f . They use $M_{\bullet} - \sigma$ relations that do not differentiate between classical and pseudo bulges. We now know (Section 6.8) that M_{\bullet} does not correlate with pseudobulges. Their BH masses are similar to those of classical bulges but scatter to lower M_{\bullet} values. The reverberation-mapped AGNs that are used to calibrate f contain a high proportion of pseudobulges. A systematic error is introduced when f is derived by comparing this sample with one that consists mostly of classical bulges. The calibration needs to be improved by classifying the (pseudo)bulges of AGN galaxies.*³ This work is in progress.

³ Graham et al. (2011) check whether barred and unbarred galaxies have different normalizations f . This is not the same as differentiating classical and pseudo bulges: some unbarred galaxies contain pseudobulges and some barred galaxies contain classical bulges (Kormendy & Kennicutt 2004). But pseudobulges are more common in barred galaxies, so Graham’s check does implicate pseudobulges. Still, so much is different in their analysis that we cannot interpret the results. For their combined (barred+unbarred) sample, they derive $f = 3.8_{-0.6}^{+0.7}$, roughly half of the canonical value. For barred AGNs only, they get $f = 2.3_{-0.5}^{+0.6}$, and for unbarred AGNs, they get $f = 7.0_{-1.4}^{+1.8}$. However, Xiao et al. (2011: Fig. 8) find no significant differences in BH masses in barred and unbarred galaxies.

S1.2. BH Masses from Single-Epoch Spectroscopy

This method was pioneered by Dibai (1977, 1984) and is sometimes known as the Dibai method (Bochkarev & Gaskell 2009; Gaskell 2009). Another name, photoionization modeling, has become a historical anachronism. Early on, the radius r used in Equation S1 was calculated by modeling the photoionization structure of the BLR (e. g., Dibai 1977, 1984; Wandel & Yahil 1985). Reverberation mapping showed that these model radii (Osterbrock & Mathews 1986) were too large by factors of ~ 10 (e. g., Gaskell & Sparke 1986; Netzer et al. 1990). Model radii have now been replaced with radii given by an observed correlation between r (from reverberation mapping) and the continuum luminosity of the AGN (Kaspi et al. 2000, 2005; Bentz et al. 2006). Correcting for contributions to the luminosity from the underlying galaxy, $r \propto L^{0.519^{+0.063}_{-0.066}}$, where L is the optical AGN luminosity conventionally measured at 5100 Å (Bentz et al. 2009a). Luminosity and emission-line width together provide M_{\bullet} , after calibration to the reverberation-mapped AGNs. An advantage of the technique is that it is inexpensive in telescope time. A single spectrum yields a mass measurement. We shall use the clumsy but accurate names “single-epoch spectroscopy mass” or “BH virial mass.”

In spite of its essentially empirical nature, single-epoch spectroscopy has become a popular tool to measure M_{\bullet} . Whereas the most widely used mass estimator, especially at low redshifts $z \lesssim 0.75$, is based on the H β line, a variety of alternatives using other lines have been developed. Greene & Ho (2005) advocate the intrinsically stronger H α line as a better choice for lower-luminosity AGNs. To help mitigate contamination from host-galaxy light, they further recommend using the H α line luminosity instead of the optical continuum luminosity to estimate the BLR size. At intermediate redshifts, $0.75 \lesssim z \lesssim 2$, McLure & Jarvis (2002) introduced a mass estimator based on Mg II $\lambda 2800$, whereas at $z \gtrsim 2$, one often has to resort to C IV $\lambda 1549$ (Vestergaard 2002). These various mass estimators have been revised and updated by Vestergaard & Peterson (2006), Wang et al. (2009), Shen et al. (2011), Xiao et al. (2011), and others. Typical uncertainties are claimed to be $\sim 0.3 - 0.5$ dex. The robustness of the rest-frame UV lines has been studied extensively (e. g., McLure & Dunlop 2004; Baskin & Laor 2005; Vestergaard & Peterson 2006; Netzer et al. 2007; McGill et al. 2008; Shen et al. 2008; Denney 2012; Ho et al. 2012; and Shen & Liu 2012). Mg II is widely viewed as an acceptable and unbiased surrogate for the Balmer lines, but many people regard C IV as potentially problematic. Fortunately, the increasing availability of near-infrared spectroscopy obviates the need to rely on the UV lines.

The virial mass method is more indirect than reverberation mapping, and it contains fewer checks that we measure virialized motions. We emphasize that application of single-epoch spectroscopy to quasars rests on the untested assumption that machinery which is calibrated for sub-Eddington BHs with $M_{\bullet} \sim 10^{7.5 \pm 1} M_{\odot}$ still works for BHs with $M_{\bullet} \sim 10^{9 \pm 1} M_{\odot}$ that radiate near the Eddington limit. In particular, work on quasars (e. g., Section 8.6) requires us to extrapolate calibrations based on local AGNs of lower L , lower M_{\bullet} , and somewhat lower $L_{\text{bol}}/L_{\text{Edd}}$. Croom (2011) argues that BLR line widths provide little additional information for quasars beyond what is given by the correlation of M_{\bullet} with quasar luminosity. More optimistically, Netzer & Marziani (2010) provide a calibration of virial masses that takes radiation pressure into account. Overall, the virial mass method is still controversial for quasars.

At the other extreme, to study the demographics of low-mass BHs (Sections 7.1–7.2), we need to extend the same mass-measurement formalism to $M_{\bullet} \approx 10^5 - 10^6 M_{\odot}$, $\sim 1 - 2$ orders of magnitude below the typical mass and luminosity of the reverberation-mapped AGNs.

S1.3. BH Masses from the X-Ray–Radio– M_{\bullet} “Fundamental Plane”

Different physics controls accretion-disk radiation at different wavelengths. So it is better news than we might expect that the correlation between radio luminosity, X-ray luminosity, and M_{\bullet} shows enough regularity so that it can be used – albeit with large uncertainties – to estimate M_{\bullet} . The correlation between L_R , L_X , and M_{\bullet} is called the “fundamental plane of BH activity” (e. g., Merloni et al. 2003; Falcke et al. 2004; KÖrding 2008; Ho 2008; Yuan et al. 2009; Hardcastle et al. 2009; Gültekin et al. 2009a). Here, we use this technique only in Section 7.3 on Henize 2-10.

BH Schwarzschild radius:

$$\begin{aligned} r_{\bullet} &= 2GM_{\bullet}/c^2 \\ &= (1.97 \text{ AU}) \frac{M_{\bullet}}{10^8 M_{\odot}} \\ &= (16.4 \text{ light min}) \frac{M_{\bullet}}{10^8 M_{\odot}}. \end{aligned}$$

Eddington luminosity:

AGN luminosity at which radiation pressure on the luminous gas is balanced by the BH gravity that holds onto this gas:

$$\begin{aligned} L_E &= \frac{4\pi G m_p}{\sigma_T} M_{\bullet} \\ &\simeq (1.26 \times 10^{46} \text{ erg s}^{-1}) \frac{M_{\bullet}}{10^8 M_{\odot}}; \end{aligned}$$

m_p is the proton mass; σ_T is the Thomson cross section for electron scattering.

Eddington ratio:

Ratio of AGN luminosity to the Eddington luminosity. Values > 1 imply that the gas is unbound and are forbidden, absent careful engineering.

S2. CLASSIFICATION CRITERIA FOR PSEUDOBULGES

The observations that are used to distinguish between classical and pseudo bulges are listed below. They are slightly refined from criteria listed in Kormendy & Kennicutt (2004) based on new data (Kormendy & Bender 2013). Justifications are given in the above reviews. For all pseudobulges listed in **Table 3**, at least two and as many as five classification criteria have been used.

1 – Pseudobulges often have disky morphology: their apparent flattening is similar to that of the outer disk, or they contain spiral structure all the way in to the center. Classical bulges are much rounder than their disks unless the galaxy is almost face-on. They cannot have spiral structure.

2 – In face-on galaxies, the presence of a nuclear bar shows that a pseudobulge dominates the central light. Bars are disk phenomena. Triaxiality in giant ellipticals involves different physics.

3 – In edge-on galaxies, boxy bulges are edge-on bars; seeing one is sufficient grounds to identify a pseudobulge. Boxy-nonrotating-core ellipticals (e. g., Kormendy et al. 2009) cannot be confused with boxy, edge-on bars, because boxy bars rotate rapidly, whereas boxy ellipticals rotate slowly.

4 – Most pseudobulges have Sérsic (1968) indices $n < 2$; almost all classical bulges have $n \geq 2$. The processes that determine Sérsic indices are not completely understood, but the correlation of small n with other pseudobulge indicators is so good that this has become a convenient classification criterion. Note, however, that some pseudobulges do have Sérsic indices as big as 4.

5 – Pseudobulges are slightly more rotation-dominated than classical bulges in the $V_{\max}/\sigma - \epsilon$ diagram; e. g., $(V_{\max}/\sigma)^* > 1$. In two-dimensional velocity fields, pseudobulges generally appear as distinct, rapidly rotating, and dynamically cold (see 6), central disk-like components.

6 – Many pseudobulges are low- σ outliers in the Faber-Jackson (1976) correlation between (pseudo)bulge luminosity and velocity dispersion, or σ decreases from the disk into the pseudobulge.

7 – If the center of the galaxy is dominated by Population I material (young stars, gas, and dust), but there is no sign of a merger in progress, then the bulge is at least *mostly* pseudo.

8 – Classical bulges fit the fundamental plane correlations for elliptical galaxies. Some pseudobulges do, too, and then these correlations are not helpful for classification. But extreme pseudobulges have larger effective radii r_e and fainter effective surface brightnesses μ_e at r_e . Also, Kormendy & Bender (2012) found some pseudobulges that are more compact than classical bulges of the same luminosity. These pseudobulges can be identified using fundamental plane correlations.

9 – Small bulge-to-total luminosity ratios do not guarantee that a bulge is pseudo, but $B/T \gtrsim 0.5$ implies that the bulge is classical.

We emphasize again that classifications are much more robust if they are based on many criteria.

S3. CORRECTIONS TO PARAMETERS LISTED IN TABLES 2 AND 3

Papers that report BH detections necessarily put great effort into estimating uncertainties in BH masses M_{\bullet} and related quantities such as bulge mass-to-light ratios. They also discuss σ because of the interest in the $M_{\bullet} - \sigma$ relation. They discuss galaxy absolute magnitudes in much less detail. Often, little information is available on the provenance and reliability of photometry and bulge-disk decompositions. However, results depend critically on the accuracy of bulge magnitudes. (Pseudo)bulge classification and bulge-disk decomposition are carried out in Kormendy & Bender (2013). Here, Section S3.1 focuses on corrections needed to get accurate apparent magnitudes. The sections that follow discuss corrections to other parameters. All these corrections are incorporated in **Tables 2** and **3**, which are reproduced from the main paper in Section S4.

S3.1. Corrections to 2MASS Apparent Galaxy Magnitudes

Almost all magnitudes used in this paper are K_s -band magnitudes (abbreviated as K) from the 2MASS sky survey (Skrutskie et al. 2006) and Large Galaxy Atlas (Jarrett et al. 2003). The reasons are well known: infrared magnitudes are less affected by dust absorption and young stars. Both are special problems for pseudobulges; indeed, ongoing star formation is one of several pseudobulge classification criteria. Luminosities are used as surrogates for stellar masses; K -band mass-to-light ratios vary little and in a calibrated way with stellar population age and color (Section 6.6.1).

Integrated magnitudes and stellar masses for (pseudo)bulge components of disk galaxies require detailed surface photometry and bulge-disk decomposition. This work for all disk galaxies with dynamical BH detections is reported in Kormendy & Bender (2013). Ellipticals are simpler: we use total magnitudes from the 2MASS Large Galaxy Atlas and the online Extended Source Catalog. These magnitudes are remarkably accurate (Jarrett et al. 2003). However, sanity checks reveal the need for small corrections in a few cases. These checks are based on V -band magnitudes, as follows:

S3.1.1 Summary A useful consistency check on V - and K -band apparent magnitudes is provided by the observation that galactic-absorption-corrected $(V - K)_0$ colors are exceedingly well behaved for almost all galaxies. Exceptions are the most internally absorbed or starbursting galaxies, but these are not relevant here. For other galaxies, we find a tight correlation between $(V - K)_0$ and $(B - V)_0$ for $0.6 \lesssim (B - V)_0 \lesssim 1.05$ (**Figure S1**). Classical bulges and ellipticals have $(V - K)_0 \simeq 2.98$ with a total scatter (not a dispersion) of about ± 0.25 . Both colors are tabulated in **Tables 2** and **3**. We use them to check the apparent magnitudes. For a few, usually faint galaxies, discrepant colors suggest that the V magnitudes in NED and Hyperleda are wrong, usually by a few tenths of a magnitude. For these, 2MASS is more accurate, and we correct the V magnitudes to make $(V - K)_0 = 2.98$. More often – usually for the largest galaxies on the sky – the 2MASS magnitudes are the problem. How we correct them is summarized here and discussed in detail in Section S3.1.2.

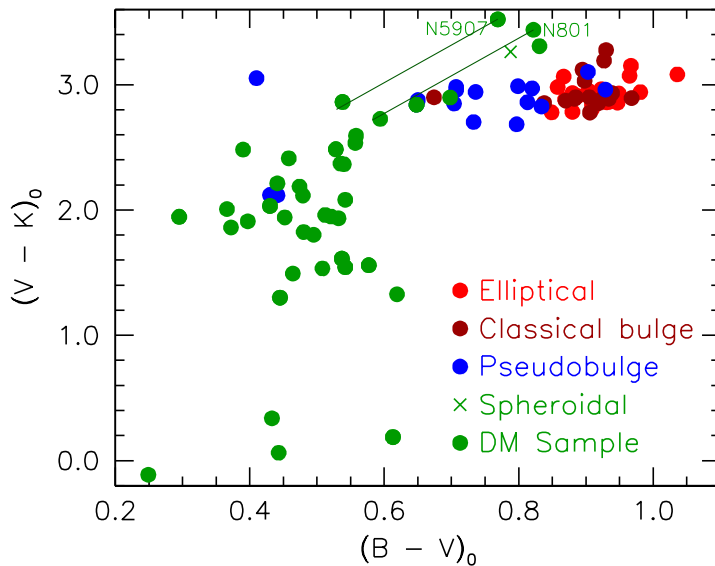


Figure S1

Correlation between Galactic-reddening-corrected, total $(B - V)_0$ and $(V - K)_0$ colors as derived by Kormendy & Freeman (2013). The ellipticals, classical bulges, and pseudobulges mostly are BH host galaxies omitting the apparently largest galaxies (M 31 and NGC 4594) and Virgo ellipticals with Sérsic indices $n \gg 4$. The filled green circles are the Sc–Im galaxies whose dark matter halos are studied by Kormendy & Freeman (2013); their large scatter at $(B - V)_0 \lesssim 0.6$ is due to a combination – details are not relevant here – of magnitude errors, heterogeneous young stellar populations, and internal absorption. The latter is illustrated for the edge-on galaxies NGC 801 and NGC 5907 by straight lines that connect the observed color values to ones that are corrected approximately for internal absorption. The unlabeled green circle with $(V - K)_0 > 3$ is NGC 253; it is very dusty and also needs correction for internal absorption. The cross is for NGC 205; it probably has an underestimated V -band luminosity. The take-away message for this paper is that $(V - K)_0$ colors are well behaved for old stellar populations. Therefore, when we observe a color that is inconsistent with the illustrated correlation (usually by being too blue), and when we trust the V -band magnitude, we correct the K -band magnitude to be consistent with the correlation.

The 2MASS photometric system is very accurate; Jarrett et al. (2003) state that the photometric zero-point calibration is accurate to 2% – 3% across the sky. To the extent that we have been able to check them (Kormendy & Bender 2013), their integrated magnitudes are correspondingly accurate at least within the radii out to which they have data. The survey is somewhat shallow; the 1-sigma sky noise is 20.0 mag arcsec⁻² in K , although profiles can be derived fainter than this by averaging over many pixels. When there is a problem, it is with the extrapolation to total magnitudes, called K_{tot} in Jarrett et al. (2003) and `k_m_ext` in the online catalog. The extrapolation is made by fitting a Sérsic function to the parts of the profile that are relatively safe from noise and from the PSF and then integrating the extrapolated function out to “about four disk scale lengths.” This procedure works best for disk galaxies, i. e., ones that have nearly exponential outer profiles. For ellipticals, the radial range is too small to yield an accurate Sérsic index (Section A2 in Kormendy et al. 2009), and their tabulated Sérsic indices are too small. The result is to underestimate the total brightnesses of ellipticals, particularly giant ellipticals that have $n \gg 4$. The derivation of this conclusion and how we correct for it are the subjects of this section.

Figure S1 shows that, when our BH hosts are not very large on the sky and when they do not have $n \gg 4$, then their $(V - K)_0$ colors are well enough behaved so that we can use them and the V magnitudes to correct the K magnitudes in problem cases. We are conservative in making this correction – we make it only when we observe a color $(V - K)_0 < 2.75$ that is much too blue. That is, if the correction is less than 0.230 mag, we do not use it. Also, in some marginal cases, it is not clear whether the V or the K magnitude is the problem. In all these cases, we use the total magnitude from 2MASS, even for ellipticals. In fact, so little is known about some of the more distant BH hosts that the 2MASS magnitudes are much more accurate than any available V -band measurements. Finally, in a few cases, our own photometry yields a composite, K -band profile with 2MASS zeropoint whose integral is more accurate than the 2MASS result because our measurements reach out to much larger radii. We adopt these total magnitudes also.

The largest correction, $\Delta K = -0.411$, is derived for M31. Jarrett et al. (2003) warn us that “The Andromeda result should be viewed with caution, as we are not fully confident that the total flux of M31 has been captured, because of the extreme angular extent of the galaxy and the associated difficulty with removing the infrared background.” This problem happens in V band, too. We adopt $V_T = 3.47 \pm 0.03$ from Walterbos & Kennicutt (1987; the error estimate is optimistic). Then the 2MASS magnitude $K = 0.984$ implies that $(V - K)_0 = 2.335$. This is much too blue for an Sb galaxy with $(B - V)_0 = 0.87$ (see **Figures S1** and **S2**). As in other such cases, we correct $K \rightarrow K - 0.411$ to make $(V - K)_0 = 2.98$ for the bulge only. The V -band bulge magnitude is determined from the V -band $B/T = 0.25 \pm 0.01$. The correction gives us a K -band magnitude for the bulge only. The infrared $B/T = 0.31 \pm 0.01$ then gives us the total observed magnitude of the galaxy, $K_T = 0.573$. Including both the red bulge and the bluer disk, the total colors of the galaxy are $(B - V)_0 = 0.87$ and $(V - K)_0 = 2.75$ (cf. **Figure S1**).

In summary, 2MASS quoted errors on K -band magnitudes, usually 0.02–0.04 mag, are most reliable for disk galaxies but can be too optimistic for giant Es. We believe that our corrected magnitudes are generally accurate to ~ 0.1 mag, although the values for M31 and for galaxies whose $(V - K)_0$ colors are very different from 2.98 are more uncertain. We quote K to higher precision because we do not wish to lose precision in arithmetic.

S3.1.2 Detailed Discussion: Dependence of K Magnitude Corrections on Sérsic Index

Two circumstances make it feasible to check K -band magnitudes using V -band magnitudes. The first is the tight correlation between $(B - V)_0$ and $(V - K)_0$ shown in **Figure S1**. Second, we have V -band total magnitudes based on detailed surface photometry for all Virgo cluster ellipticals from Kormendy et al. (2009, hereafter KFCB). These are more thoroughly checked and should be more accurate than other photometry in the literature. KFCB conservatively estimate errors in total magnitudes as ± 0.07 mag for ellipticals with Sérsic (1968) index $n < 4$ and ± 0.10 for those with $n > 4$. The agreement with Hyperleda is actually better than this. KFCB paid particular

attention to the extrapolation of V_T to infinite radius, so these data allow us to look for faint outer light that may have been missed by 2MASS. How we do this is illustrated in **Figures S2** and **S3**.

Figure S2 correlates $(V - K)_0$ color with $(B - V)_0$ color and galaxy apparent magnitude V_T . Here, K_T is from 2MASS and V_T is from KFCB for the green points and, in order of preference, from Kormendy & Bender (2013), Hyperleda, or RC3 otherwise. The right-hand panels are designed to compare $(V - K)_0$ to a raw observational parameter that should contain little physics but that can easily correlate with measurement errors. But first, we need to check whether $(V - K)_0$ correlates with stellar population age using the more sensitive indicator $(B - V)_0$ in the left panels. Ellipticals have only a small range in $(B - V)_0$ color (panel *a*). Bulges show a large range (panel *c*), mostly in pseudobulges, and bluer pseudobulges live in galaxies that are bluer overall (Drory & Fisher 2007). Over this wide range in $(B - V)_0$, (pseudo)bulges show remarkably little variation in $(V - K)_0$, consistent with the shallow correlation shown at $0.6 \lesssim (B - V)_0 \lesssim 1.05$ in **Figure S1**. In contrast, ellipticals have a large range in $(V - K)_0$, and this results from the fact that $(V - K)_0$ correlates with V_T (panel *b*). Note that, unlike **Figure S1**, **Figure S2** does not omit large-Sérsic-index ($n \gg 4$) galaxies. This suggests that the large range in $(V - K)_0$ color for ellipticals is not a stellar population effect but rather is a result of a measurement problem.

KFCB total magnitudes V_T were tested thoroughly and agree with Hyperleda to 0.06 mag with a slight dependence on Sérsic index n . We therefore conclude that the correlation of the green points in **Figure S2b** signals a problem with the K magnitudes. The black points for BH host galaxies share this correlation with almost the same scatter: the problem is not V for them, either. As noted above, 2MASS could have trouble with sky subtraction for large galaxy images or trouble in adding up the faint outer light in very shallow brightness profiles. Importantly, the problem is not shared by disk galaxies: panel *d* shows no significant correlation. Because disks have steep outer profiles ($n \simeq 1$) whereas bright ellipticals have shallow profiles ($n > 4$), the hint is that the problem is associated with profile shape. This is confirmed in **Figure S3**.

The exceptions among bulges are M31 and the Sombrero Galaxy, NGC 4594. In both galaxies, $(B - V)_0$ is normal, but $(V - K)_0$ is very discrepant. The problem with M31 is its large apparent size (see Section S3.1.1). The problem with NGC 4594 is that it, too, has a large apparent diameter, and moreover, it is bulge-dominated with large n at large radii. We therefore correct the total K magnitudes for these two galaxies.

Returning to the ellipticals, we need to further investigate the correlation in **Figure S1b** in order to decide how we should correct their K_T magnitudes. If the problem is mainly galaxy size as measured by V_T , then we should assume that all bright- V_T galaxies need correction, and we should carry out that correction using the fit shown by the green line in panel *b*. On the other hand, if the problem is associated with Sérsic index, then we should use either n or the discrepant $(V - K)_0$ color but not V_T to determine which galaxies to correct.

If profile shape n affects the measurement of K_T and hence $(V - K)_0$, then we might expect that n is a “second parameter” which controls the scatter about the correlation in **Figure S2b**. **Figure S3a** confirms that this is the case. Largely independent of V_T (which is encoded in symbol size), deviations $\Delta(V - K)_0$ from the correlation in **Figure S2b** correlate with n . Galaxies with larger n (that is, shallower outer profiles) have more negative deviations, i. e., smaller $(V - K)_0$. Therefore, if V magnitudes are not a problem and if all bulges have approximately the same color, then more negative $\Delta(V - K)_0$ implies that the K_T magnitudes are too faint. There are a few exceptions. Two of these galaxies are faint and difficult for 2MASS. In particular, VCC 1627 is the faintest known elliptical in Virgo; it is less luminous than M32. The point for NGC 4636 is correct; we checked the 2MASS and KFCB magnitudes. The KFCB and Hyperleda total magnitudes V_T agree to 0.01 mag. So a few exceptions are real. But by and large, our suspicions are confirmed: the problem with K_T magnitudes happens mostly for large- n galaxies.

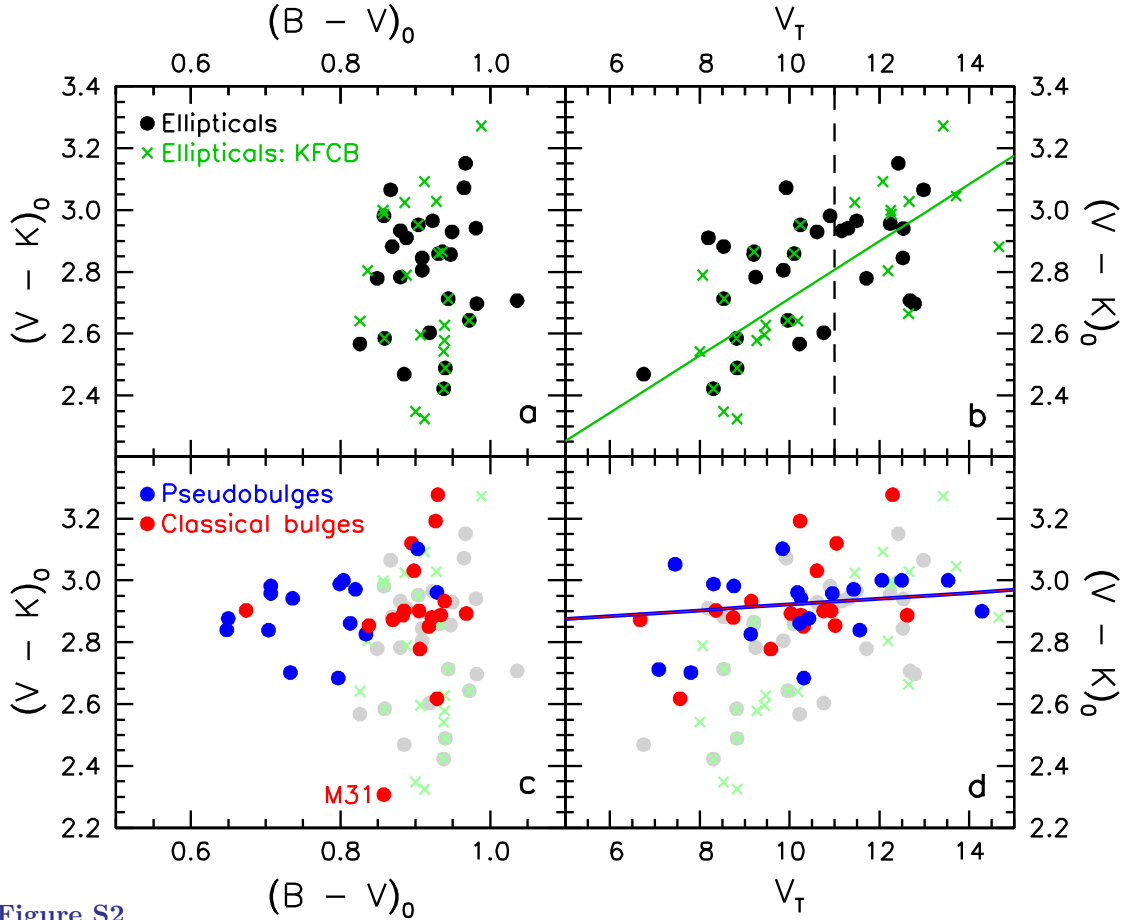
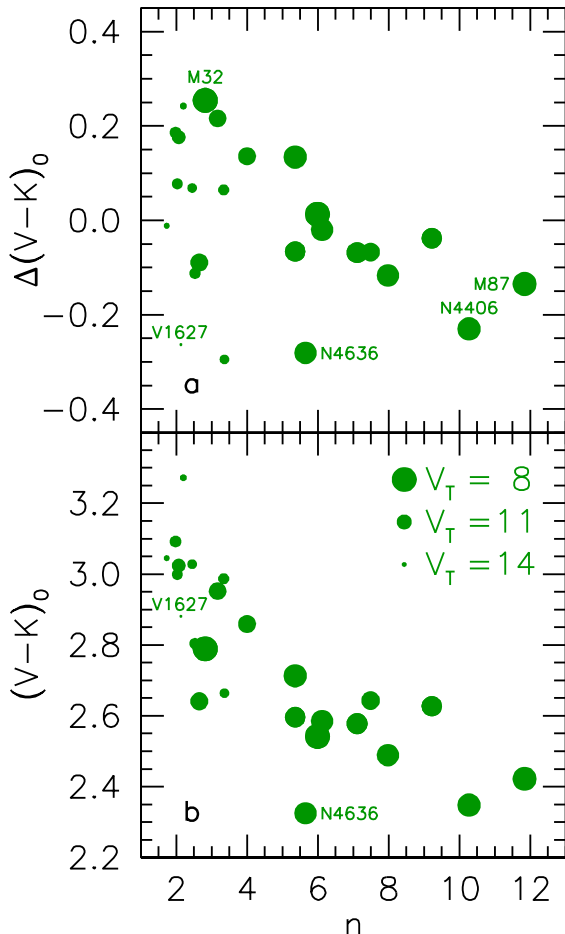


Figure S2

Correlations of total galaxy $(V - K)_0$ color with (*left*) total $(B - V)_0$ color and (*right*) total apparent magnitude V_T . Subscript 0 means that colors are corrected for Galactic absorption (Schlegel et al. 1998). The upper panels are for ellipticals; the lower panels are for classical and pseudo bulges. The green points are for galaxies from Kormendy et al. (2009: KFCB). Other points are for BH host galaxies, eight of which are also in KFCB. The ellipticals are repeated in ghostly light colors in the lower panels to facilitate comparison. In panel *b*, the green line is a least-squares fit to the KFCB points assuming negligible errors in V_T . The RMS deviations of the green points about this line and the RMS deviations of the black points about a similar fit (*not illustrated*) to the BH Es are both 0.16 mag. These deviations correlate with galaxy Sérsic index (**Figure S3a**). For this reason, and because $(V - K)_0$ does not vary systematically over the small $(B - V)_0$ color range shown, we argue that both the panel *b* trend with V_T and much of the scatter about this trend result either from sky subtraction errors in the apparently largest galaxies or from errors in adding up faint surface brightnesses over large areas in ellipticals with shallow profiles (large n). **Figure S3** shows that n is the primary factor. We therefore correct the 2MASS K_T magnitudes for galaxies with $(V - K)_0 < 2.75$ to the mean color for KFCB galaxies with $V_T > 11$ (*vertical dashed line*), $\langle (V - K)_0 \rangle = 2.98 \pm 0.05$. In panel *d*, the red and blue line is a least-squares fit to the classical and pseudo bulges; RMS = 0.13 mag. They show no significant trend of $(V - K)_0$ with $(B - V)_0$ or V_T and have the same mean $(V - K)_0$ color as the faint ellipticals. In the lower panels, only the brightest galaxy M31 ($V_T = 3.5$) and the bright, bulge-dominated galaxy NGC 4594 have very anomalously blue colors. We correct only their K -band magnitudes to make $(V - K)_0 = 2.98$.

**Figure S3**

(a) Correlation of the $(V - K)_0$ deviations of the green points from the green line in **Figure S2b** versus the Sérsic index n of the elliptical galaxy’s brightness profile. Point sizes are linearly proportional to apparent magnitude V_T (see the key). Some points are labeled with galaxy names. With few exceptions (mostly faint galaxies but also NGC 4636), K brightnesses are underestimated with respect to the correlation – i. e., $\Delta(V - K)_0$ is negative – by larger amounts for ellipticals that have shallower outer brightness profiles (larger n). This suggests that n is the main factor that controls the $(V - K)_0 - V_T$ correlation in **Figure S2b**. This is confirmed here in panel *b*. Even the tiniest Virgo elliptical, VCC 1627, which is an exception in *a*, participates in the strong correlation in *b*. Thus n and not image area (represented by V_T) is the primary factor that controls the K -band magnitude errors. We therefore correct K_T and M_K for BH ellipticals in **Figure S2** that have $(V - K)_0 < 2.75$ until their colors agree with the mean color $\langle (V - K)_0 \rangle = 2.98 \pm 0.05$ for bright ellipticals in **Figure S2b** or for ellipticals with small n in panel *b* here.

Large- n galaxies are also the most luminous galaxies (KFCB). The range of distances represented in **Figure S2** is not very large; among green points, it is especially small. Therefore V_T is not too different from M_{V_T} . This opens up the possibility that the whole correlation in **Figure S2b** and not just the scatter is caused mainly by the 2MASS response to different n . **Figure S3b** confirms that this is the case. There is a very good, nonlinear correlation between $(V - K)_0$ and n such that galaxies with larger n have K -band luminosities that are more underestimated. This correlation has substantially smaller scatter than the one in **Figure S2b**. VCC 1627 is no longer discrepant. We emphasize: 2MASS photometry of apparently fainter galaxies is usually excellent. The errors uncovered in **Figures S2** and **S3** are mostly < 0.2 to 0.5 mag, and they apply mainly to the biggest giant ellipticals and to M31. Painstaking, deep photometry was required in KFCB to measure the outer profiles of Virgo giant ellipticals. It is not surprising that the somewhat shallow 2MASS survey misses some outer light in these large and shallow-surface-brightness-gradient galaxies.

A related, more pessimistic discussion of 2MASS galaxy magnitude errors is in Schombert (2011).

The above results suggest a practical strategy for correcting the K -band magnitudes on which many of our results depend. We cannot make corrections based on Sérsic indices, because these have not reliably been measured for most BH ellipticals. But the black and green points behave very similarly in **Figure S2**. The faint, non-Virgo BH ellipticals that have anomalously blue colors also are giant ellipticals. We therefore correct K_T for ellipticals that have $(V - K)_0 \leq 2.75$ to make their resulting colors equal the mean color $\langle (V - K)_0 \rangle = 2.98 \pm 0.05$ for the faint KFCB ellipticals in **Figure S2**. That is, we correct ellipticals if their colors are “too blue” by ~ 1.5 sigma or more. These corrections are included in **Tables 2** and **3** in the main paper and below.

S3.2. Corrections to Stellar Dynamical BH Masses for Core Galaxies

Gebhardt & Thomas (2009), Shen & Gebhardt (2010), Schulze & Gebhardt (2011), and Rusli et al. (2013) demonstrate convincingly that stellar dynamical mass models that do not include dark matter halos underestimate M_\bullet by factors that can be as large as 2 or more when the BH sphere of influence is not well resolved. The effect is small for coreless galaxies; we neglect it when models that include dark matter are not available. Fortunately, almost all stellar dynamical M_\bullet estimates for core galaxies are now based on models that include dark matter. For one exception, NGC 5576, we correct M_\bullet as discussed in the notes on individual objects. For NGC 3607, the correction is too uncertain and we omit the object (table notes; orange point in **Figure 12**).

S3.3. Corrections to Effective Velocity Dispersions

This section enlarges on Section 5.1 in the main paper. **Figure 11** is reproduced from there.

The velocity dispersion σ_e that we correlate with M_\bullet is more heterogeneously defined in different papers and less consistently measured within these definitions than we usually suppose. This is a stealth “can of worms” that could be a bigger problem than the more obvious uncertainties in BH mass measurements that preoccupy authors. We check values when we can and fix a few problems. But the necessary data are not available for all objects. Fortunately, we can show that this problem is not too severe.

The worries are these:

1. *A priori*, we do not know how best to define σ_e so that we learn important physics from the $M_\bullet - \sigma_e$ correlation. Clearly we should not include data at $r \lesssim r_{\text{infl}}$ in the average. But inside what fraction of r_e should we average $\sigma(r)$? We usually claim that we average inside r_e and call the result σ_e . However:
2. Accurate values of r_e are known for only a few galaxies. KFCB demonstrate via high-dynamic-range photometry that brightness profiles of giant ellipticals extend farther out than we have thought. The r_e values derived in KFCB are more accurate than previous results, and they are larger than previous values for almost all giant ellipticals. We use them here. But we do not have such data for most BH hosts. It is safe to assume that the r_e values in common use are too small. For bulges, the situation has been worse. Accurate decompositions have been available for only a few galaxies. As part of the writing of this review, they are being derived for the remaining disk-galaxy BH hosts in Kormendy & Bender (2013).
3. Different fractions of r_e are used by different authors. For example, Ferrarese & Merritt (2000) use $r_e/8$, whereas the Nuker team uses r_e .
4. Different authors perform the radial averaging differently. We follow the Nuker team practice (e.g., Pinkney et al. 2003; Gültekin et al. 2009c) and use $\sigma_e^2 = \text{average of } V(r)^2 + \sigma(r)^2$, weighting by $I(r)dr$. Usually, we adopt σ_e from the M_\bullet source paper or from Gültekin et al. (2009c). When we calculate it, we perform the average inside $r_e/2$, because our r_e values tend to be larger than those in the literature, and we wish to be consistent with published σ_e values. When we recalculate σ_e , we include a comment in the notes on individual objects.

However (Section 5.1 of the main paper), our practice can be contrasted with σ_e values from the SAURON team: They add spectra that sample the galaxy in two dimensions inside r_e or inside the SAURON field, whichever is smaller (Emsellem et al. 2007). Because σ and V rather than $\sigma^2 + V^2$ are averaged and because the weighting of different radii is essentially by $2\pi r I(r)dr$ rather than by $I(r)dr$, the resulting σ_e values are smaller than the ones that we use. *No study has proved that the Nuker definition produces a tighter $M_\bullet - \sigma_e$ correlation or that a tighter correlation is more meaningful physically.* However, because it is most commonly used and therefore most widely available, we use the Nuker definition here.

In view of these concerns, it is prudent to check how much our results might depend on the definition of σ_e or on how well its measurement follows that definition. **Figure 11** (reproduced from the main paper for the convenience of readers) compares our σ_e values with central velocity dispersions tabulated in HyperLeda and with σ_e values calculated as described above by the SAURON/ATLAS3D team. We conclude that adopting either alternative would have minimal effect on the scatter in the $M_\bullet - \sigma_e$ correlation and essentially no effect on qualitative conclusions.

HyperLeda includes a few bad measurements. These are particularly expected for pseudobulges, which can have small dispersions that are undersampled by low wavelength resolution. Pseudobulge dispersion measurements can also have serious problems with dust and star formation. But it is relatively easy to find and discard these problems and get improved central σ values that should agree with our σ_e values as well as do the velocity dispersions of classical bulges and ellipticals.

SAURON/ATLAS3D σ_e values mostly agree very well with ours. Some SAURON values are smaller, as expected. But conclusions would not be changed if we had SAURON σ_e values for all galaxies.

Important: The average shift $\Delta \log \sigma_e = \log(\text{Nuker } \sigma_e) - \log(\text{SAURON } \sigma_e) = 0.0299$ or a factor of 1.07 will be relevant in Section 8 when we compare the $z \simeq 0$ $M_\bullet - \sigma_e$ relation with ones derived for galaxies at large redshifts. All high- z observations necessarily add spectra (not $V^2 + \sigma^2$ values) inside apertures that are large in kpc. The SAURON σ_e values are the closest match at $z \simeq 0$. We therefore use the above factor to correct our least-squares fit to the local $M_\bullet - \sigma_e$ correlation when we make comparisons to high- z objects.

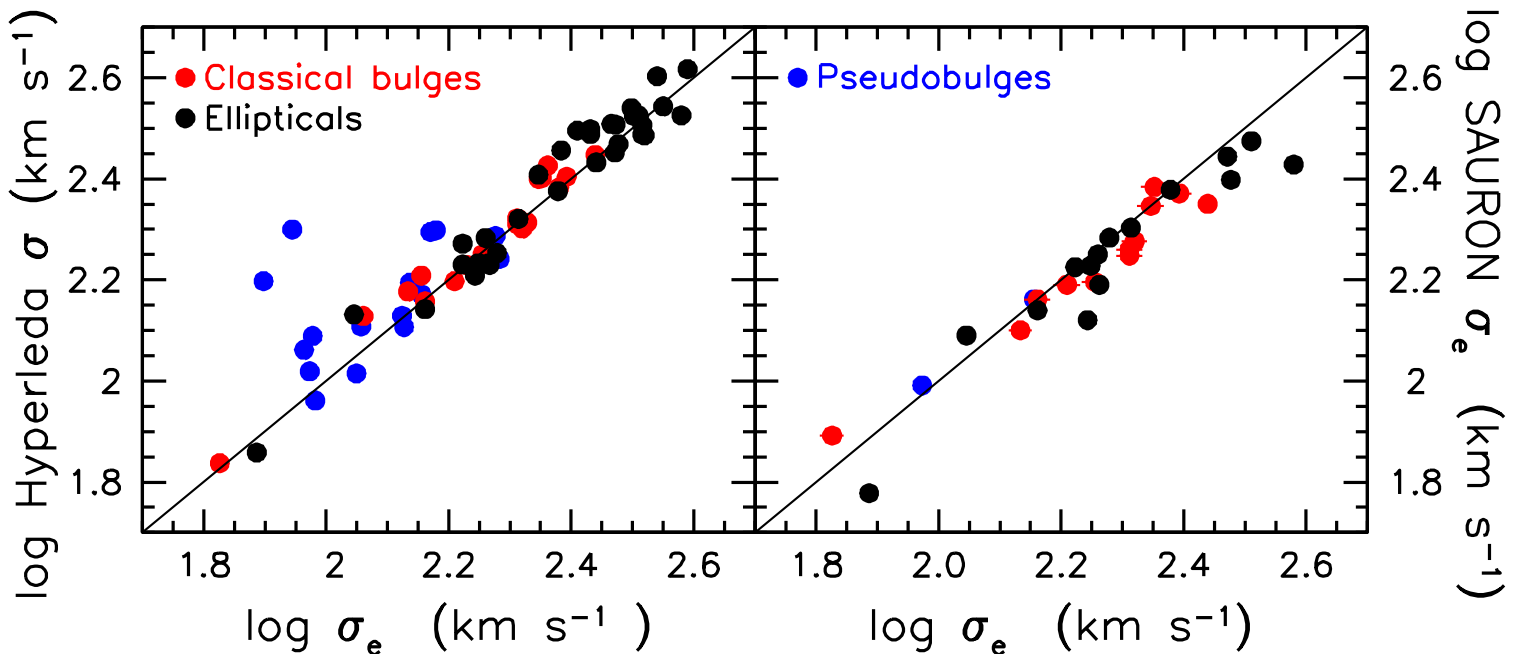


Figure 11

Comparison of our adopted σ_e (Tables 2 and 3) to (left) the central velocity dispersion as tabulated in HyperLeda and to (right) the σ_e value tabulated by the SAURON/ATLAS3D teams (Emsellem et al. 2007; Cappellari et al. 2013). The straight lines are not fits; they indicate equality. Given our definition, it is reassuring that our σ_e is approximately the geometric mean of the HyperLeda central and SAURON/ATLAS3D σ_e values.

S4. BH DATABASE

This section reproduces essentially verbatim the first part of Section 5 in the main paper. Its purpose is to include the notes to **Tables 2** and **3**. For the convenience of readers, we do not fragment the discussion by including the tables only in the main text and the notes (except for brief examples) only here. Rather, we include all of main paper Section 5 to the end of the table notes.

This section is an inventory of galaxies that have BH detections and M_\bullet measurements based on spatially resolved stellar dynamics, ionized gas dynamics, CO molecular gas disk dynamics, or maser disk dynamics. **Table 2** lists ellipticals, including mergers-in-progress that have not yet relaxed into equilibrium. **Table 3** lists disk galaxies with classical bulges (upper part of table) and pseudobulges (lower part of table). The demographic results discussed in Sections 6–9 of the main paper are based on these tables. Both tables are provided in machine-readable form in the electronic edition of this paper.

We review the M_\bullet measurements in Sections 2 and 3 of the main paper. This Supplemental Material provides more detail. It includes all the notes on individual objects in Sections S4.1–S4.4. Derivations of host galaxy properties are relatively straightforward for ellipticals. They are more complicated for disk-galaxy hosts, because (pseudo)bulge classification is crucial and because (pseudo)bulge–disk photometric decomposition is necessary. This work is too long to fit here; it is published in a satellite paper written in parallel with this review (Kormendy & Bender 2013). Some details are repeated here in the table notes for the convenience of readers.

Implicit in the tables are decisions about which published M_\bullet measurements are reliable enough for inclusion. No clearcut, objective dividing line separates reliable and questionable measurements. Our decisions are personal judgments. Our criteria are similar to those in Gültekin et al. (2009c); when we made a different decision, this is explained in the notes on individual objects. We try to be conservative. With a few exceptions that are not included in correlation fits, stellar dynamical masses are retained only if they are based on three-integral models. Nevertheless (Section 3), it is likely that systematic errors – e.g., due to the neglect of triaxiality in giant ellipticals – are still present in some data. For this reason, we do not discuss correlation scatter in much detail. We do, however, include the important conclusion that the intrinsic scatter in the correlation of M_\bullet with bulge stellar mass is as small as the intrinsic scatter in the correlation of M_\bullet with σ . And we derive the most accurate correlations that we can with present data (Section 6.6).

The sources of the adopted M_\bullet measurements are given in the last column of each table, and earlier measurements are discussed in the notes on individual objects. The M_\bullet error bars present a problem, because different authors present error bars with different confidence intervals. For consistency, we use approximate one-sigma standard deviations, i.e., 68% confidence intervals. When authors quote two-sigma or three-sigma errors, we follow Krajnović et al. (2009) and estimate that one-sigma errors are N times smaller than N -sigma errors. Flags in Column 12 of **Table 2** and Column 19 of **Table 3** encode the method used to determine M_\bullet , whether the galaxy has a core (ellipticals only), and whether M_\bullet was derived with models that include triaxiality or dark matter and large orbit libraries. Only the models of M 32, NGC 1277, and NGC 3998 include all three.

We use a distance scale (Column 3) based mainly on surface brightness fluctuation measurements at small distances and on the WMAP 5-year cosmology at large distances ($H_0 = 70.5 \text{ km s}^{-1} \text{ Mpc}^{-1}$; Komatsu et al. 2009). Details are in the notes that follow **Tables 2** and **3**. Velocity dispersions σ_e (Columns 11 and 17 of **Tables 2** and **3**) are problematic; they are discussed in Section S3.3.

We discuss luminosity correlations only in terms of K_s -band absolute magnitudes. However, we also provide V magnitudes for the convenience of readers and because we use them to check the K_s magnitudes. Readers should view $(B-V)_0$ as a galaxy color that contains physical information but $(V-K_s)_0$ mainly as a sanity check of the independent V and K_s magnitude systems (Section S3.1). Our K_s magnitudes are on the photometric system of the Two Micron All Sky Survey (2MASS; Skrutskie et al. 2006); the effective wavelength is $\sim 2.16 \mu\text{m}$. To good approximation, $K_s = K - 0.044$ (Carpenter 2001; Bessell 2005), where K is essentially Johnson’s (1962) 2.2 μm bandpass. Except in Section S3.1, in this paragraph, and in the tables, we abbreviate K_s as K for convenience. **Tables 2** and **3** list K_s apparent magnitudes of the galaxies from the 2MASS Large Galaxy Atlas (Jarrett et al. 2003) or from the online Extended Source Catalog. Corrections (usually a few tenths of a mag) have been made for some of the brightest or angularly largest galaxies as discussed in Section S3.1.

Table 2 Supermassive black holes detected dynamically in 44 elliptical galaxies

Galaxy	Type	Distance (Mpc)	K_s	M_{KsT}	M_{VT}	$(V-K_s)_0$	$(B-V)_0$	$\log M_{\text{bulge}}$ (M_\odot)	M_\bullet (low M_\bullet – high M_\bullet) (M_\odot)	σ_e (km s^{-1})	Flags M C M_\bullet	Source
(1)	(2)	(3)	(4)	(5)	(6)	(7)	(8)	(9)	(10)	(11)	(12)	(13)
M 32	E2	0.805 7	5.10	-19.45	-16.64	2.816	0.895	9.05 ± 0.10	$2.45(1.43-3.46) \times 10^6$	77 ± 3	1 0 1	van den Bosch + 2010
NGC 1316	E4	20.95 1	5.32	-26.29	-23.38	2.910	0.871	11.84 ± 0.09	$1.69(1.39-1.97) \times 10^8$	226 ± 9	1 0 0	Nowak + 2008
NGC 1332	E6	22.66 2	7.05	-24.73	-21.58	3.159	0.931	11.27 ± 0.09	$1.47(1.27-1.68) \times 10^9$	328 ± 9	1 0 0	Rusli + 2011
NGC 1374	E0	19.57 1	8.16	-23.30	-20.43	2.874	0.908	10.65 ± 0.09	$5.90(5.39-6.51) \times 10^8$	167 ± 03	1 0 1	Rusli 2012,Rusli+2013
NGC 1399	E1	20.85 1	6.31	-25.29	-22.43	2.863	0.948	11.50 ± 0.09	$8.81(4.35-17.81) \times 10^8$	315 ± 03	1 1 0	see notes
NGC 1407	E0	29.00 2	6.46	-25.87	-22.89	2.980	0.969	11.74 ± 0.09	$4.65(4.24-5.38) \times 10^9$	276 ± 2	1 1 1	Rusli 2012,Rusli+2013
NGC 1550	E1	52.50 9	8.77	-24.87	-21.89	2.974	0.963	11.33 ± 0.09	$3.87(3.16-4.48) \times 10^9$	270 ± 10	1 1 1	Rusli 2012,Rusli+2013
NGC 2778	E2	23.44 2	9.51	-22.34	-19.39	2.955	0.911	10.26 ± 0.09	$1.45(0.00-2.91) \times 10^7$	175 ± 8	1 0 1	Schulze + 2011
NGC 2960	E2	67.1 9	9.78	-24.36	-21.30	3.068	0.880	11.06 ± 0.09	$1.08(1.03-1.12) \times 10^7$	166 ± 16	3 0 0	Kuo + 2011
NGC 3091	E3	53.02 9	8.09	-25.54	-22.56	2.980	0.962	11.61 ± 0.09	$3.72(3.21-3.83) \times 10^9$	297 ± 12	1 1 1	Rusli 2012,Rusli+2013
NGC 3377	E5	10.99 2	7.16	-23.06	-20.08	2.980	0.830	10.50 ± 0.09	$1.78(0.85-2.72) \times 10^8$	145 ± 7	1 0 1	Schulze + 2011
NGC 3379	E1	10.70 2	6.27	-23.88	-21.01	2.867	0.939	10.91 ± 0.09	$4.16(3.12-5.20) \times 10^8$	206 ± 10	1 1 1	van den Bosch + 2010
NGC 3607	E1	22.65 2	6.99	-24.79	-21.92	2.872	0.911	11.26 ± 0.09	$1.37(0.90-1.82) \times 10^8$	229 ± 11	1 1 0	Gültekin + 2009b
NGC 3608	E1	22.75 2	7.62	-24.17	-21.19	2.980	0.921	11.01 ± 0.09	$4.65(3.66-5.64) \times 10^8$	182 ± 9	1 1 1	Schulze + 2011
NGC 3842	E1	92.2 9	8.84	-25.99	-23.01	2.980	0.941	11.77 ± 0.09	$0.09(6.28-11.43) \times 10^9$	270 ± 27	1 1 1	McConnell+2011a,2012
NGC 4261	E2	32.36 2	6.94	-25.62	-22.64	2.980	0.974	11.65 ± 0.09	$5.29(4.21-6.36) \times 10^8$	315 ± 15	2 1 0	Ferrarese + 1996
NGC 4291	E2	26.58 2	8.42	-23.72	-20.76	2.954	0.927	10.85 ± 0.09	$9.78(6.70-12.86) \times 10^8$	242 ± 12	1 1 1	Schulze + 2011
NGC 4374	E1	18.51 1	5.75	-25.60	-22.62	2.980	0.945	11.62 ± 0.09	$9.25(8.38-10.23) \times 10^8$	296 ± 14	2 1 0	Walsh + 2010
NGC 4382	E2	17.88 1	5.76	-25.51	-22.53	2.980	0.863	11.51 ± 0.09	$1.30(0.00-22.4) \times 10^7$	182 ± 5	1 1 0	Gültekin + 2011
NGC 4459	E2	16.01 1	7.15	-23.88	-20.91	2.975	0.909	10.88 ± 0.09	$6.96(5.62-8.29) \times 10^7$	167 ± 8	2 0 0	Sarzi + 2001
NGC 4472	E2	16.72 1	4.97	-26.16	-23.18	2.980	0.940	11.84 ± 0.09	$2.54(2.44-3.12) \times 10^9$	300 ± 7	1 1 1	Rusli 2012,Rusli+2013
NGC 4473	E5	15.25 1	7.16	-23.77	-20.89	2.874	0.935	10.85 ± 0.09	$0.90(0.45-1.35) \times 10^8$	190 ± 9	1 0 1	Schulze + 2011
M 87	E1	16.68 1	5.27	-25.85	-22.87	2.980	0.940	11.72 ± 0.09	$6.15(5.78-6.53) \times 10^9$	324^{+28}_{-12}	1 1 1	Gebhardt + 2011
NGC 4486A	E2	18.36 1	9.49	-21.83	-18.85	2.980	...	10.04 ± 0.09	$1.44(0.92-1.97) \times 10^7$	111 ± 5	1 0 0	Nowak + 2007
NGC 4486B	E0	16.26 1	10.39	-20.67	-17.69	2.980	0.991	9.64 ± 0.10	$6. (4. - 9.) \times 10^8$	185 ± 9	1 0 0	Kormendy + 1997
NGC 4649	E2	16.46 1	5.49	-25.61	-22.63	2.980	0.947	11.64 ± 0.09	$4.72(3.67-5.76) \times 10^9$	380 ± 19	1 1 1	Shen+Gebhardt 2010
NGC 4697	E5	12.54 1	6.37	-24.13	-21.33	2.799	0.883	10.97 ± 0.09	$2.02(1.52-2.53) \times 10^8$	177 ± 8	1 0 1	Schulze + 2011
NGC 4751	E6	32.81 2	8.24	-24.38	-21.22	3.158	0.983	11.16 ± 0.09	$1.71(1.52-1.81) \times 10^9$	355 ± 14	1 0 1	Rusli 2012,Rusli+2013
NGC 4889	E4	102.0 9	8.41	-26.64	-23.63	3.007	1.031	12.09 ± 0.09	$2.08(0.49-3.66) \times 10^{10}$	347 ± 5	1 1 1	McConnell+2011a,2012
NGC 5077	E3	38.7 9	8.22	-24.74	-21.66	2.949	0.987	11.28 ± 0.09	$8.55(4.07-12.93) \times 10^8$	222 ± 11	2 1 0	De Francesco + 2008
NGC 5128	E	3.62 6	3.49	-24.34	-21.36	2.980	0.898	11.05 ± 0.09	$5.69(4.65-6.73) \times 10^7$	150 ± 7	1 1 0	Cappellari + 2009
NGC 5328	E2	64.4 9	8.49	-25.58	-22.61	2.966	1.004	11.65 ± 0.09	$4.75(2.81-5.63) \times 10^9$	333 ± 2	1 1 1	Rusli + 2013
NGC 5516	E3	55.3 9	8.31	-25.47	-22.50	2.970	0.993	11.60 ± 0.09	$3.69(2.65-3.79) \times 10^9$	328 ± 11	1 1 1	Rusli 2012,Rusli+2013
NGC 5576	E3	25.68 2	7.83	-24.23	-21.29	2.939	0.862	11.00 ± 0.09	$2.73(1.94-3.41) \times 10^8$	183 ± 9	1 1 0	Gültekin + 2009b
NGC 5845	E3	25.87 2	9.11	-22.97	-19.73	3.238	0.973	10.57 ± 0.09	$4.87(3.34-6.40) \times 10^8$	239 ± 11	1 0 1	Schulze + 2011
NGC 6086	E	138.0 9	9.97	-25.74	-22.84	2.884	0.965	11.69 ± 0.09	$3.74(2.59-5.50) \times 10^9$	318 ± 2	1 1 1	McConnell + 2011b
NGC 6251	E1	108.4 9	9.03	-26.18	-23.18	2.998	...	11.88 ± 0.09	$6.14(4.09-8.18) \times 10^8$	290 ± 14	2 1 0	Ferrarese + 1999
NGC 6861	E4	28.71 2	7.71	-24.60	-21.42	3.179	0.962	11.25 ± 0.09	$2.10(2.00-2.73) \times 10^9$	389 ± 3	1 0 1	Rusli 2012,Rusli+2013
NGC 7052	E3	70.4 9	8.57	-25.70	-22.86	2.841	0.86	11.61 ± 0.10	$3.96(2.40-6.72) \times 10^8$	266 ± 13	2 1 0	van der Marel + 1998
NGC 7619	E3	53.85 2	8.03	-25.65	-22.83	2.821	0.969	11.65 ± 0.09	$2.30(2.19-3.45) \times 10^9$	292 ± 5	1 1 1	Rusli 2012,Rusli+2013
NGC 7768	E4	116.0 9	9.34	-26.00	-23.19	2.811	0.906	11.75 ± 0.09	$1.34(0.93-1.85) \times 10^9$	257 ± 26	1 1 1	McConnell + 2012
IC 1459	E4	28.92 2	6.81	-25.51	-22.42	3.081	0.966	11.60 ± 0.09	$2.48(2.29-2.96) \times 10^9$	331 ± 5	1 0 0	Cappellari + 2002
IC 1481	E1.5	89.9 9	10.62	-24.17	$1.49(1.04-1.93) \times 10^7$...	3 0 0	Huré + 2011
A1836 BCG	E	152.4 9	9.99	-25.95	-22.64	3.310	1.043	11.81 ± 0.10	$3.74(3.22-4.16) \times 10^9$	288 ± 14	2 1 0	Dalla Bontá + 2009
A3565 BCG	E	49.2 9	7.50	-25.98	-23.03	2.948	0.956	11.78 ± 0.09	$1.30(1.11-1.50) \times 10^9$	322 ± 16	2 1 0	Dalla Bontá + 2009
Cygnus A	E	242.7 9	10.28	-26.77	-23.23	3.54	$2.66(1.91-3.40) \times 10^9$	270 ± 90	2 1 0	Tadhunter + 2003

Column 1 is the galaxy name; BCGs are brightest cluster galaxies in the Abell clusters named. Purple listings are not included in fits (Section 6.3). Column 2 is Hubble type (mostly RC3). Green lines are for mergers in progress (Section 6.4). If only M_\bullet is purple, we accept it but do not include it in the correlation fits (see Section 6.6). Column 3 is the assumed distance from the following sources, starting with the highest-priority sources:

- (1) Blakeslee et al. (2009) surface-brightness fluctuation (SBF) distances for individual galaxies in the Virgo and Fornax clusters;
- (2) Tonry et al. (2001) SBF corrected via Equation A1 in Blakeslee et al. (2010);
- (3) Mei et al. (2007) SBF mean distance to the Virgo W' cloud (de Vaucouleurs 1961);
- (4) Mei et al. (2007) SBF mean distance to the Virgo cluster (no W' cloud);
- (5) Thomsen et al. (1997) SBF distance to NGC 4881 in the Coma cluster;
- (6) mean of distance determinations adopted in Kormendy et al. (2010); sources are given there;
- (7) Monachesi et al. (2011); agrees with (8);
- (8) mean of many determinations listed on NED, using mainly SBF distances and those based on Cepheid, TRGB, and RR Lyrae stars.
- (9) As a last resort, we adopt D (Local Group) given by NED for the recession velocity of the galaxy (if isolated) or its group (if in a group or cluster) and for the WMAP 5-year cosmology parameters (Komatsu et al. 2009).
- (10) van den Bosch et al. (2012).

Column 4 is the 2MASS K_s total magnitude. When $(V-K_s)_0 = 2.980$ in Column 7, K_s has been corrected as discussed in Section S3.1. Columns 5 and 6 are the K_s - and V -band absolute magnitudes based on the adopted distances and Galactic absorption corrections from Schlegel et al. (1998) as recalibrated by Schlafly & Finkbeiner (2011). The V -band magnitudes are taken, in order of preference, from KFCB, from RC3, or from Hyperleda (usually “integrated photometry” but sometimes the main table if it implies a more realistic $(V-K_s)_0$ color).

Columns 7 and 8 are the $V-K_s$ and $B-V$ colors of the galaxy corrected for Galactic reddening.

Column 9 is the base-10 logarithm of the bulge mass (Section 6.6.1).

Column 10 is the measured BH mass with 1-sigma range in parentheses from sources in Column 13.

Column 11 is the stellar velocity dispersion σ_e . We adopt the usual convention that σ_e^2 is the intensity-weighted mean of $V^2 + \sigma^2$ out to a fixed fraction of the effective radius r_e that contains half of the light of the galaxy. As discussed briefly in Section 5.1 of the main paper and in more detail in Section S3.3 here, we adopt $r_e/2$ when we calculate σ_e from photometry and published kinematics (see notes on individual objects). When no note is given, σ_e is from the M_\bullet source paper or from Gültekin et al. (2009c).

Column 12 lists three flags: “M” encodes the method used to measure M_\bullet , using 1 for stellar dynamics, 2 for ionized gas dynamics, and 3 for maser dynamics. “C” = 1 implies that the galaxy has a core (e.g., Lauer et al. 1995). “ M_\bullet ” = 1 implies that the BH mass has been “corrected” by making dynamical models that include large orbit libraries and triaxiality (M 32 and NGC 3379) or dark matter halos.

S4.1. Notes on Individual Elliptical Galaxies

M32: The BH discovery papers and history of M_\bullet measurements are discussed in §2.2.1. We adopt M_\bullet from the triaxial models of van den Bosch & de Zeeuw (2010). We calculate $\sigma_e = 77 \pm 3 \text{ km s}^{-1}$ from our photometry ($r_e/2 = 38''/2$) and kinematics in Simien & Prugniel (2002). The value averaged inside r_e is 1 km s^{-1} smaller. This is in good agreement with $\sigma_e = 75 \pm 3 \text{ km s}^{-1}$ in Tremaine et al. (2002), Gültekin et al. (2009c), and McConnell & Ma (2013). In contrast, Graham & Scott (2013) adopt $\sigma_e = 55 \text{ km s}^{-1}$, in part because they do not include $V(r)$.

NGC 2778, NGC 3608, NGC 4291, NGC 4473, NGC 4649, NGC 4697, and NGC 5845: The BH discovery is by Gebhardt et al. (2003).

NGC 1316: This galaxy is bluer than the typical giant E, with $(B-V)_0 = 0.87$ (NED). Based on our experience with published total magnitudes of bright galaxies (e.g., KFCB), we adopt $B_T = 9.17$ from the Hyperleda integrated photometry table. This yields $M_{VT} = -23.38$. The 2MASS $K = 5.587$ magnitude then implies that $(V-K)_0 = 2.64$. This is implausible for $(B-V)_0 = 0.871$, indicating that the K luminosity is underestimated. We use the $(V-K)_0$ versus $(B-V)_0$ correlation to derive $(V-K)_0 = 2.91$ and hence to correct the K magnitude by -0.268 magnitudes to $K = 5.319$. This is a typical correction for a nearby giant elliptical.

NGC 1332 and NGC 4751: These galaxies initially presented us with an interpretation dilemma. We believe that it is solved and that both galaxies are best interpreted as (rather extreme) ellipticals. However, realizing this required us to learn something new about elliptical galaxies. This note explains our conclusions and summarizes the consequences of the more canonical alternative that these are S0 galaxies.

Both galaxies are highly flattened (E6) and contain prominent, almost-edge-on nuclear dust disks. It is remarkable how many BH host ellipticals contain nuclear dust disks: NGC 1332, NGC 3379 (faintly), NGC 3607, NGC 4261, NGC 4374, NGC 4459, NGC 4486A and NGC 5845 (in which much of the nuclear gas disk has formed stars), NGC 4697, NGC 4751, NGC 6251, NGC 6861, NGC 7052, NGC 7768, A1836 BCG, A3565 BCG, and probably IC 1459. Several more contain nuclear disks of stars that plausibly formed out of gas-and-dust disks in the manner illustrated by NGC 4486A (Kormendy et al. 2005) and NGC 5845 (Lauer et al. 1995). Of course, this does not prove that all these objects – especially NGC 1332 and NGC 4751 – are ellipticals; bona fide S0₃ galaxies contain nuclear dust disks, too (e.g., NGC 5866 in the *Hubble Atlas*, Sandage 1961). One reason why dust-lane E and S0 galaxies are preferentially found among BH hosts is that seeing a dust lane motivates authors to measure an emission-line rotation curve. The prevalence of central gas disks in BH hosts is interesting from a BH feeding point of view, but their importance in this note is that they tell us that NGC 1332 and NGC 4751 are almost edge-on.

Images of NGC 1332 and NGC 4751 suggest that both galaxies contain two components, a central one that is relatively round and that has a steep brightness gradient and an outer one that looks flatter and that has a shallower brightness gradient. These are defining features of S0 galaxies. If the central component is interpreted as a bulge and the outer one as a disk, then plausible decompositions are possible and give $B/T = 0.43$ for NGC 1332 (Rusli et al. 2011) and $B/T = 0.55 \pm 0.05$ for NGC 4751 (Kormendy & Bender 2013). We emphasize: *If these interpretations are correct, then NGC 1332 closely resembles the S0 galaxies NGC 1277 and MGC 4342 in having a bulge that contains an abnormally high-mass BH (see Figure 15 for illustration). NGC 4751 is similar but less extreme. Like NGC 1277 and NGC 4486B, both galaxies then also have high velocity dispersions that are well outside the scatter in the Faber-Jackson (1976) correlation between E or bulge luminosity and velocity dispersion. That is, if NGC 1332 and NGC 4751 are S0s, then they are further examples of the high- M_\bullet BH monsters discussed in Section 6.5.*

However, a compelling argument suggests that these galaxies are extremely flattened extra-light ellipticals:

KFCB present and review evidence that Virgo cluster ellipticals are naturally divided into two kinds, $M_{VT} < -21.6$ galaxies that have cores and $M_{VT} \geq -21.5$ galaxies that have central extra light above the inward extrapolation of the outer $n \simeq 3 \pm 1$ Sérsic-function main body (see Sections 6.7 and 6.13 in the main paper). They suggest that and (e.g.) Hopkins et al. (2009) model how extra-light ellipticals form in wet mergers, such that the main body of the galaxy is the scrambled-up remnant of the pre-merger disk and bulge stars and the extra-light component is manufactured by a starburst during the merger. In Virgo ellipticals, the fraction of the stellar mass that is in the extra-light component is $\sim 5\%$ (if just the extra light is counted: KFCB) or a few 10s of percents (if a standard Sérsic-Sérsic decomposition is applied: Hopkins et al. 2009). Both kinds of ellipticals are represented among our BH hosts; NGC 3377 and NGC 4459 are typical extra-light ellipticals.

Huang et al. (2013) make a similar study of ellipticals in field environments. They show that field ellipticals are different from cluster ellipticals in three ways that are relevant here: (1) extra light (their “two inner components”) makes up a larger fraction $\sim 20\%$ to 40% of the galaxies, (2) extra-light ellipticals extend to higher luminosities in the field than in the Virgo cluster, and (3) field ellipticals can be as flat as E6 (their Figure 1). In the context of these results, NGC 1332 and NGC 4751 are more plausibly interpreted as extra-light ellipticals, not S0s. In fact, even though NGC 1332 is exceedingly close to edge-on, its isophotes are more rectangular than those of an edge-on thin disk; this motivated Sandage & Bedke (1994) to emphasize (their italics) that the galaxy contains a “thick disk”.

We now believe that there may be almost a continuum in the properties (although not a seamless overlap in numbers) of outer bodies of these galaxies from E5 ellipticals with a modest amount of extra light (NGC 3377) to E6 ellipticals that are roughly half extra light (NGC 4751 and NGC 6861) to E6 galaxies whose outer parts resemble thickened disks (NGC 1332) to true S0s with thin disks (NGC 5866). Objects like NGC 4751 and NGC 1332 may be rare, and it appears that they are confined to the field, perhaps because this environment favors formation by a small number of gentle mergers that involve progenitors with large gas fractions. This is the interpretation of NGC 1332 and NGC 4751 that we adopt when we construct BH correlation diagrams and least-squares fits. **Figure 15** illustrates both interpretations for NGC 1332.

NGC 1399: As discussed in Section 3.1, we adopt the mean M_\bullet measured by Houghton et al. (2006) and by Gebhardt et al. (2007). Conservatively, we adopt $1\text{-}\sigma$ errors that span the complete range obtained in both measurements. Also, $\sigma_e = 315 \text{ km s}^{-1}$ is calculated using kinematic data from Graham et al. (1998), intensity-weighting $V^2 + \sigma^2$ out to $0.5r_e = 56''$ using our photometry.

NGC 2778 had a BH detection in Gebhardt et al. (2003) but only a M_\bullet upper limit in Schulze & Gebhardt (2011). However, $M/L_K = 3.3$ is too big for an old stellar population minus dark matter, implying that the M_\bullet limit is too small. We illustrate it in **Figure 12** and then omit it.

NGC 2960: The BH discovery paper is Henkel et al. (2002); a reliable BH mass was determined by Kuo et al. (2011). NGC 2960 has frequently been classified as Sa? (RC3, UGC, NED), but Kormendy & Bender (2013) and **Figure 13** in the main paper show that it is a merger in progress. The galaxy is therefore listed here, with the ellipticals. The dispersion is from Greene et al. (2010).

NGC 3377: The BH was found by Kormendy et al. (1998), whose measurements $M_\bullet = (2.1 \pm 0.9) \times 10^8 M_\odot$ and $M/L_V = 2.0 \pm 0.2$ agree well with $M_\bullet = (1.9 \pm 1.0) \times 10^8 M_\odot$ and $M/L_V = 2.3 \pm 0.4$ in Schultze & Gebhardt (2011). The reasons are (1) that the resolution of the CFHT spectroscopy was very good, (2) that the assumption by Kormendy of an isotropic velocity distribution in this low-luminosity, extra-light (Kormendy 1999), and rapidly rotating (Emsellem et al. 2004) elliptical was close enough to the truth, and (3) that this E5 galaxy is essentially guaranteed to be edge-on. The BH mass in NGC 3377 was also measured in Gebhardt et al. (2003). The 2MASS K -band magnitude gives an implausible color of $(V-K)_0 = 2.69$. We have corrected K_s in **Table 2** to give the mean color for giant ellipticals, $(V-K)_0 = 2.980$.

NGC 3379 is a core elliptical with dynamical models that include triaxiality (the only core galaxy that has such models) but not dark matter (van den Bosch & de Zeeuw 2010). However, the HST FOS spectra (Gebhardt et al. 2000b) resolve the BH sphere of influence with $r_{\text{infl}}/\sigma_* \simeq 7.1$. Schulze & Gebhardt (2011) and Rusli et al. (2013) show that M_\bullet does not require a significant correction for dark matter under these circumstances.

NGC 4374 (M84) is the fifth-brightest elliptical in the Virgo cluster, but it is only 0.61 mag fainter than NGC 4472 (KFCB). Like many radio galaxies, it (3C 272.1) has a nuclear gas and dust disk (Bower et al. 1997) which makes it feasible to search for a BH relatively independently of the stellar mass distribution (Walsh, Barth & Sarzi 2010) by measuring the emission-line gas rotation curve. NGC 4374 is the first galaxy in which a BH discovery was made using HST STIS (Bower et al. 1998). STIS’s long-slit capability made it possible to see the prominent zig-zag in the emission lines that is the signature of the BH.

However, as discussed in Section 3.2, the line profile is complicated by a two-component structure, and this has led to some uncertainty in M_\bullet . Bower et al. (1998) decompose the line profiles into slowly- and rapidly-rotating components and use the latter to get $M_\bullet = 1.63(0.99-2.83) \times 10^9 M_\odot$. Maciejewski & Binney (2001) suggest that the complicated line profile is caused by integrating the light of the nuclear disk inside a spectrograph slit that is broader ($0''.2$ wide) than the telescope PSF. They estimate $M_\bullet = 4.4 \times 10^8 M_\odot$. The large difference between these two determinations has been a cause of concern, not only for NGC 4374 but also for other M_\bullet determinations based on emission lines. Recently, Walsh, Barth & Sarzi (2010) model the observations in much greater detail and – importantly – include the effects of the velocity dispersion in the gas. After application of this “asymmetric drift” correction, they get $M_\bullet = 9.25(8.38 - 10.23) \times 10^8 M_\odot$. We adopt their value but note (§ 3.2) that there are still significant uncertainties in emission-line M_\bullet measurements. *The folklore that gas rotation curves give M_\bullet easily and without the complications and uncertainties inherent in stellar dynamical modeling is much too optimistic.*

NGC 4382: The Gültekin et al. (2011) M_\bullet limit is based on stellar dynamical models that do not include dark matter. For $M_\bullet \leq 1.3_{-1.2}^{+5.2} \times 10^7 M_\odot$, $r_{\text{infl}}/\sigma_* \simeq 0.3$ is not well resolved. Since this is a core galaxy, we need to ask whether an upward correction to the M_\bullet limit is required. Examination of Gültekin’s analysis suggests that no correction is needed: (1) The core is unusually small (break radius $r_b = 81$ pc, Lauer et al. 2005) for the high luminosity of the galaxy. Our only BH host E that has a smaller $r_b = 54$ pc in Lauer et al. (2005) is NGC 3608, for which Schulze & Gebhardt (2011) find the same M_\bullet with and without dark matter. (2) The kinematic measurements analyzed by Gültekin only reach $0.28 r_e$, i.e., the inner part of the galaxy that is most dominated by visible matter. Large M_\bullet corrections in Schulze et al. (2011) happen when the ground-based observations reach larger fractions of r_e . In confirmation, (3) Gültekin et al. (2011) remark: “Within ~ 2 kpc, about the outer extent of our data, [Nagino & Matsushita 2009, who] study the gravitational potential as revealed by X-ray emission from the interstellar medium, ... find a constant B -band mass-to-light ratio consistent with a potential dominated by stellar mass.” We therefore use Gültekin’s BH mass limit in **Figure 14**. However, the Table 2 listing includes in the upper error bar a (probably too conservative) correction for the inclusion of halo dark matter.

NGC 4459 is the second-brightest extra-light elliptical in the Virgo cluster and the brightest one that has Sérsic $n < 4$ ($n = 3.2 \pm 0.3$; KFCB). Therefore – as indicated by the normal color, $(V - K)_0 = 2.975$ – the 2MASS K_T magnitude is accurate. The galaxy has a prominent nuclear dust disk; in this sense, it closely resembles NGC 1332, NGC 4751, and many other BH host ellipticals discussed in the notes to those objects.

M 87: The early history of BH searches is reviewed in KR95. We consider the BH discovery paper to be the HST gas-dynamical study by Harms et al. (1994). They derived $M_\bullet = (2.7 \pm 0.8) \times 10^9 M_\odot$ (all masses are corrected to the SBF distance of 16.68 Mpc; Blakeslee et al. 2009). For many years, the definitive mass measurement – also based on HST gas kinematics – was $M_\bullet = (3.6 \pm 1.0) \times 10^9 M_\odot$ (Macchetto et al. 1997). Stellar dynamical measurement of M_\bullet is difficult, because the central brightness profile is shallow inside the break radius $r_b = 5''.66$ that defines the “core” (Lauer et al. 1992, 2007). The result (Kormendy 1992a, b) is unfavorably small luminosity weighting inside the BH sphere of influence, $r_{\text{infl}} \simeq 3''.1$. Even a steep central increase in $\sigma(r)$ is strongly diluted by projection. Measuring LOSVDs helps if one can detect the resulting high-velocity wings (van der Marel 1994b). M 87 remains too expensive for HST absorption-line spectroscopy, but high- S/N ground-based spectroscopy is successful. Gebhardt & Thomas (2009) fit a variety of kinematic measurements, including two-dimensional spectroscopy from SAURON (Emsellem et al. 2004) and higher-resolution, long-slit spectroscopy from van der Marel et al. (1994a; seeing FWHM = $0''.6$; slit width = $1''$). They for the first time include dark matter in the dynamical models; this is important because the tradeoff in mass between dark and visible matter inevitably decreases the measured stellar mass-to-light ratio at large radii. Analysis machinery is still based on the assumption that M/L is independent of radius, so the consequence is to reduce M/L near the center, too. To maintain a good fit to the kinematics, M_\bullet must be increased. Gebhardt & Thomas (2009) derive $M/L_V = 10.9 \pm 0.4$ and $M_\bullet = (2.1 \pm 0.6) \times 10^9 M_\odot$ without including dark matter and $M/L_V = 6.8 \pm 0.9$ and $M_\bullet = (6.0 \pm 0.5) \times 10^9 M_\odot$ including dark matter. The change is in the expected sense. Recently, Gebhardt et al. (2011) add Gemini telescope integral-field spectroscopy aided by laser-guided AO; the resulting PSF has a narrow core (FWHM = $0''.06$) that contributes 14–45% of the PSF light. Such good resolution allows a substantial improvement in the reliability of the BH mass measurement. They get and we adopt $M_\bullet = 6.15(5.78 - 6.53) \times 10^9 M_\odot$.

As in many other galaxies in which stellar- and gas-dynamical M_\bullet measurements can be compared, the stellar dynamical mass is substantially larger. In M 87, it is a factor of 1.74 ± 0.50 larger than the Macchetto et al. (1997) value. Such comparisons are discussed further in Section 3.2.

NGC 4486A: This galaxy has a bright star $2''.5$ from its center that affects most published magnitude measurements. KFCB measure the total $V_T = 12.53$ magnitude without this star, and this provides $M_{VT} = -18.85$. The 2MASS magnitude appears to include the star, so we do not use it. Instead, we adopt the well determined $(V - K)_0 = 2.980$ color for old elliptical galaxies and derive $M_{KT} = -21.83$ from M_{VT} . For M_\bullet , we read $1\text{-}\sigma$ error bars from the χ^2 contour diagram in Figure 6 of Nowak et al. (2007).

NGC 4486B is one of the lowest-luminosity, normal ellipticals known. The most accurate photometry (KFCB) gives $V_T = 13.42$ and, with the present distance, $M_{VT} = -17.69$. M 32 is about 1 mag fainter. Again, we adopt $(V - K)_0 = 2.980$ in preference to the 2MASS K magnitude to get $M_{KT} = -20.67$. The BH mass $M_\bullet \simeq 6.1_{-2.0}^{+3.0} \times 10^8 M_\odot$ is the only one based on spherical, isotropic stellar dynamical models that we use in this paper. We use it (1) because the central velocity dispersion $\sigma = 291 \pm 25$ km s $^{-1}$ is much larger than the upper envelope $\sigma \sim 160$ km s $^{-1}$ (for the galaxy’s luminosity) of the scatter in the Faber-Jackson (1976) correlation. As in the case of NGC 1277 (q. v.), this is a strong indicator of unusually high masses, even though anisotropic models can formally fit the data without a BH. However, we have already noted that low-luminosity, coreless ellipticals (e.g., M 32) are not generally very anisotropic. NGC 4486B is a rapid rotator. (2) We do not use M_\bullet in any correlation fits. Instead, we include NGC 4486B as the earliest discovery of a compact, early-type galaxy which deviates from the M_\bullet -host-galaxy correlations in the direction of abnormally high M_\bullet . The most extreme such galaxy is NGC 1277 (**Table 3** and **Figure 15**).

NGC 5077: We use the BH mass that was calculated including emission-line widths in the analysis (De Francesco et al. 2008, see p. 361) and adopt the corresponding high- M_\bullet error bar. The low- M_\bullet error bar is from the analysis that does not include line widths.

NGC 5128: At a distance of 3.62 Mpc, NGC 5128 = Centaurus A is the second-nearest giant elliptical (after Maffei 1 at 2.85 Mpc) and the nearest radio galaxy. It is therefore very important for the BH search. It is also a merger-in-progress, although that merger may be relatively minor. It will prove to be important to our conclusion in Section 6.4 that mergers-in-progress often have BH masses that are small compared to expectations from the M_\bullet -host-galaxy correlations.

The problem is that the many published M_\bullet measurements show big disagreements (Section 3.2). Five measurements based on the rotation of a nuclear gas disk are available. In recent years, as measurements and modeling have improved, the mass measurements have converged reasonably well: We have

$M_\bullet = 2.07(0.62 - 5.18) \times 10^8 M_\odot$ (Marconi et al. 2001) based on ESO VLT observations without AO;

$M_\bullet = 1.14(0.60 - 1.24) \times 10^8 M_\odot$ (Marconi et al. 2006) based on HST STIS spectroscopy and including uncertainties from the poorly constrained inclination of the gas disk in the error bars;

$M_\bullet = 0.63(0.55 - 0.69) \times 10^8 M_\odot$ (Håring-Neumayer et al. 2006) based on VLT with AO and including the gas velocity dispersion in the estimate;

$M_\bullet = 0.85(0.71 - 0.93) \times 10^8 M_\odot$ (Krajinović, Sharp, & Thatte 2007) based on Gemini telescope spectroscopy without AO; the Pa β rotation curve is consistent with zero velocity dispersion; and

$M_\bullet = 0.47(0.43 - 0.52) \times 10^8 M_\odot$ (Neumayer et al. 2007) based on VLT SINFONI spectroscopy with AO; the gas dispersion is taken into account. The convergence of M_\bullet measurements based on gas dynamics is reassuring. However, two stellar dynamical measurements agree poorly:

$M_\bullet = 2.49(2.28 - 2.80) \times 10^8 M_\odot$ (Silge et al. 2005) based on Gemini observations without AO, and

$M_\bullet = 0.57(0.47 - 0.67) \times 10^8 M_\odot$ (Cappellari et al. 2009) based on VLT SINFONI spectroscopy with AO.

The last set of measurements has the highest resolution and S/N , and it agrees with the latest gas-dynamical results. We adopt this M_\bullet .

NGC 5576: This is a core elliptical (Lauer et al. 2007) with a BH detection and M_\bullet measurement in Gültekin et al. (2009b). Halo dark matter was not included in the dynamical models, but the resolution $r_{\text{infl}}/\sigma_* = 3.3$ is good enough so that we can apply a correction calibrated by Schulze & Gebhardt (2011) and by Rusli et al. (2013). The mean of the two corrections is a factor of 1.6 ± 0.3 . We applied this correction and added the uncertainty in the correction to the uncertainty in Gültekin’s M_\bullet measurement in quadrature to give the estimated 1- σ error quoted in the table.

NGC 6861 is classified as an S0₃ galaxy in Sandage & Tammann (1981) because of its prominent nuclear dust disk. Méndez-Abreu et al. (2008) estimate that $B/T \simeq 0.64$. However, our photometry shows little or no significant departure from an $n \simeq 2$ Sérsic-function main body with central extra light. That is, the galaxy is similar to NGC 4459, another extra-light elliptical (KFCB) with a central dust disk that motivated an S0₃ classification in Sandage & Tammann (1981). There could be a faint disk component in NGC 6861 such as the one in NGC 3115; if so, it makes no difference to any conclusions in this paper. We therefore classify the galaxy as an extra-light elliptical.

IC 1459: The BH discovery by Verdoes Kleijn et al. (2000) is based on HST WFPC2 photometry, HST FOS spectroscopy through six apertures to measure the emission-line rotation curve, and ground-based, CTIO 4 m telescope spectroscopy with FWHM $\sim 1''/9$ seeing to measure the stellar kinematics. They get $M_\bullet \sim (5 \text{ to } 7) \times 10^9 M_\odot$ from stellar dynamical modeling but $M_\bullet \sim (0.2 \text{ to } 0.7) \times 10^9 M_\odot$ from the HST gas dynamics. In contrast, Cappellari et al. (2002) combine HST STIS spectroscopy with high- S/N ground-based spectroscopy (CTIO 4 m telescope; seeing FWHM $\approx 1''/5$; slit width = $1''/5$; CCD scale = $0''/73 \text{ pixel}^{-1}$) that provide both emission-line and absorption-line kinematics. Again, the agreement between gas and star measurements is not superb: stellar dynamics give $M_\bullet = 2.48(2.29 - 2.96) \times 10^9 M_\odot$ (which we adopt), whereas gas dynamics give $M_\bullet \approx 3.34 \times 10^9 M_\odot$. As noted in §3.2, the comparison between gas and stellar dynamics is not reassuring.

At $r \leq 43''/2 = r_e/2$, we measure $\sigma_e = 329 \text{ km s}^{-1}$ from the kinematic data in Cappellari et al. (2002) and $\sigma_e = 332 \text{ km s}^{-1}$ from the kinematic data in Samurović & Danziger (2005). We adopt $\sigma_e = 331 \pm 5 \text{ km s}^{-1}$. The data reach far enough out to measure a value inside r_e ; this would be only 2.6 km s^{-1} smaller than the value that we adopt. Our photometry shows that this is an extra-light elliptical with $n \simeq 3.1^{+0.4}_{-0.3}$.

IC 1481: The BH discovery paper is Mamyoda et al. (2009). They detect maser sources distributed along a line indicative of an edge-on molecular disk, and they see a symmetrical rotation curve. But $V(r) \propto r^{-0.19 \pm 0.04}$ is substantially sub-Keplerian. They conclude that the maser disk is more massive than the BH. Huré et al. (2011) present an analysis method that is suitable for a wide range of disk-to-BH mass ratios. They measure $M_\bullet = (1.49 \pm 0.45) \times 10^7 M_\odot$ and a maser disk mass of about $4.1 \times 10^7 M_\odot$ (see §3.3.3, where these values are quoted for the distance $D = 79 \text{ Mpc}$ adopted by Huré). We adopt these values.

The host galaxy is illustrated in **Figure 13**. SDSS images show loops, shells, and dust lanes characteristic of a major merger in progress. The overall light distribution is that of a normal extra-light elliptical with Sérsic $n = 2.5^{+0.25}_{-0.2}$. Consistent with this, the central $2'' \times 2''$ of the galaxy has an A-F, post-starburst spectrum (Bennert, Schulz & Henkel 2004). The ellipticity profile shows that this object is turning into an E1.5 elliptical, so we list it in **Table 2**. In Section 6.4, we include it among mergers in progress.

S4.2. Notes on Individual Disk Galaxies with Classical Bulges

M31: The BH mass measurements are discussed in §2. We adopt M_\bullet determined from P3, the blue cluster part of the triple nucleus (Bender et al. 2005). We recomputed $\sigma_e = 169 \pm 8 \text{ km s}^{-1}$ from our photometry and kinematic data in Saglia et al. (2010). Integrating to r_e or $r_e/2$ gives the same result. The agreement with $\sigma_e = 160 \pm 8 \text{ km s}^{-1}$ in Gültekin et al. (2009c) is good. Chemin, Carignan, & Foster (2009) provide V_{circ} .

Photometry is difficult, because the galaxy is large. The V - and K -band magnitudes are discussed in Section S3.1.1 (see also **Figure S2**) as an example of the correction of 2MASS magnitudes. Since our BH correlations are derived in K band, we use an infrared measurement of the bulge-to-disk ratio. Kormendy & Bender (2013) measure $B/T = 0.31 \pm 0.03$ in L band (**Table 3** here). This agrees with the mean of four, L -band measurements by Seigar, Barth & Bullock (2008), Tempel, Tamm & Tenjes (2010), Kormendy et al. (2010), and Courteau et al. (2011). However, $B/T = 0.25 \pm 0.02$ is smaller in V band, and we use this smaller value in deriving the V -band bulge and disk magnitudes.

M81: The BH discovery and $M_\bullet = 6 (\pm 20\%) \times 10^7 M_\odot$ measurement are reported in Bower et al. (2000). There are two concerns: this result is based on axisymmetric, two-integral stellar dynamical models, and it has never been published in a refereed journal. Also, Devereux et al. (2003) measure M_\bullet using HST STIS spectroscopy to get the ionized gas rotation curve; the problems here are that the [N II] emission lines are blended with and had to be extracted from broad H α emission and that the width of the [N II] emission lines is not discussed. But, whereas the danger is that the emission-line rotation curve will lead us to underestimate M_\bullet , Devereux et al. (2003) get $M_\bullet = 7(6 - 9) \times 10^7 M_\odot$, larger than Bower’s value. Both measurements are problematic, but they agree. Also, Bower’s measurement of M_\bullet in NGC 3998 in the same abstract agrees with a reliable stellar dynamical measurement in Walsh et al. (2012). So we adopt the average of the Bower and Devereux M_\bullet measurements.

Available B/T measurements in the visible and infrared agree within errors. We adopt the mean $B/T = 0.34 \pm 0.02$ (Kormendy & Bender 2013).

NGC 524: Krajnović et al. (2009) use $\sigma_e = 235 \text{ km s}^{-1}$ from Emsellem et al. (2007), but this is from a luminosity-weighted sum of spectra inside r_e . It is therefore not consistent with the Gültekin et al. (2009c) definition. For consistency, we computed $\sigma_e = 247 \text{ km s}^{-1}$ from kinematic data in Simien & Prugniel (2000) and our photometry.

NGC 821, NGC 3384, NGC 4564, and NGC 7457: The BH discovery is by Gebhardt et al. (2003).

NGC 821 is usually considered to be an elliptical galaxy, but the shapes of the isophotes in the image in the *Carnegie Atlas of Galaxies* (Sandage & Bedke 1994) suggests that it is an almost-edge-on S0. In fact, Scorza & Bender (1995) did a bulge-disk decomposition and got $B/T = 0.943$. Kormendy & Bender (2013) collect V -band photometry; they get $V_T = 10.96$ and $B/T = 0.969$. We adopt $B/T = 0.95$ here. We emphasize that no conclusions depend on B/T or on our reclassification of the galaxy as an S0. The bulge Sérsic index is ~ 4.9 ; under these circumstances, it is commonly necessary to correct the 2MASS K_T magnitude slightly. We determine a correction of $\Delta K_T = -0.185$ and apply it to derive the photometric parameters listed in **Table 3**.

NGC 1023: The asymptotic outer rotation velocity $V_{\text{circ}} = 251 \pm 15 \text{ km s}^{-1}$ is from Column (12) of Table 1 in Dressler & Sandage (1983).

NGC 1277: We adopt the Perseus cluster distance and NGC 1277 BH mass from van den Bosch et al. (2012). However, our analysis of the host galaxy (Kormendy & Bender 2013) is different from that of van den Bosch, who decomposes the light distribution into four radially overlapping components. This is operationally analogous to a multi-Gaussian expansion in the sense that it forces the Sérsic indices of all components to be small. Partly for this reason, they concluded that the bulge is not classical. We find that the ellipticity at large radii is similar to the ellipticity near the center; this is a sign also seen in many edge-on S0s in the Virgo cluster (Kormendy & Bender 2012) and indicates that the bulge dominates at both small and large radii. We decomposed the galaxy into two components such that the bulge dominates at both small and large radii. The decomposition is robust, the bulge has a Sérsic index of 3.5 ± 0.7 , and $B/T = 0.55 \pm 0.07$. Both results imply that the bulge is classical.

NGC 2549: Krajnović et al. (2009) find that $M_\bullet = (1.4^{+0.2}_{-1.3}) \times 10^7 M_\odot$ for $D = 12.3 \text{ Mpc}$, quoting 3- σ errors. In this case, dividing the 3- σ error bars by 3 would obscure the fact that this is an unusually weak BH detection. We therefore read the 1- σ errors directly from the χ^2 contours shown in their paper. The result is approximate, $M_\bullet = 1.45(0.31 - 1.65) \times 10^7 M_\odot$ for our adopted $D = 12.70 \text{ Mpc}$, but more realistic.

NGC 3115: Kormendy & Richstone (1992) discovered the BH and got $M_\bullet = 1.0(0.3 - 3.3) \times 10^9 M_\odot$ from isotropic models and a smallest possible $M_\bullet = 1 \times 10^8 M_\odot$ from the most extreme anisotropic model that fit their CFHT kinematic data. These are consistent with $M_\bullet = 0.90(0.62 - 0.95) \times 10^9 M_\odot$ adopted from Emsellem, Dejonghe & Bacon (1999). Additional measurements have ranged from $5 \times 10^8 M_\odot$ to $2 \times 10^9 M_\odot$ (Kormendy et al. 1996b; Magorrian et al. 1998).

NGC 3585: The outer rotation velocity V_{circ} for the embedded disk is from Scorza & Bender (1995).

NGC 3998 is listed twice in **Table 3**, once with the BH mass that we adopt from stellar dynamical models (Walsh et al. 2012) and once with the smaller BH mass based on the emission-line rotation curve (De Francesco et al. 2006). We illustrate this in **Figure 12** as an example of why we do not use M_\bullet values that are determined from ionized gas rotation curves when line widths are not taken into account.

We use $B/T = 0.85 \pm 0.02$ from bulge-disk decompositions in Kormendy & Bender (2013) and in Sánchez-Portal et al. (2004). With this B/T , NGC 3998 is the most significant bulge outlier to the $M_\bullet - M_{K,\text{bulge}}$ correlation, as Walsh et al. (2012) concluded. There is a possibility that a three-component, bulge-lens-disk decomposition is justified; if so, B/T would be smaller, ~ 0.66 . Then NGC 3998 would be a more significant outlier, in the manner of NGC 4342 and the galaxies discussed in Section 6.5. For σ_e , we adopt the mean of $\sigma_e = 270 \text{ km s}^{-1}$ found by Walsh for $r_e \simeq 18''$ from our photometry and $\sigma_e = 280 \text{ km s}^{-1}$ which we find using Gültekin’s definition, our photometry, and kinematic data from Fisher (1997).

NGC 4258: The discovery paper for the spectacular H_2O maser disk and consequent accurate BH mass measurement is Miyoshi et al. (1995). Herrnstein et al. (1999) uses the masers to measure a direct geometric distance $D = 7.2 \pm 0.3 \text{ Mpc}$ to NGC 4258. Herrnstein et al. (1999) interpret small departures from precise Keplerian rotation in terms of a warped gas disk and derive an improved BH mass. Our adopted mass is based in large part on this result. Section 3.3 provides the details. Sources for V_{circ} are listed in Kormendy et al. (2010).

Given a “bomb-proof” accurate BH mass in a conveniently inclined galaxy, NGC 4258 has been used to test both stellar dynamical and ionized-gas-dynamical M_\bullet measurement machinery (Sections 3.1 and 3.2, respectively).

NGC 4526: This is the brightest S0 galaxy in the Virgo cluster and the first galaxy to have a BH discovered using the central CO rotation curve (Davis et al. 2013). We use $B/T = 0.65 \pm 0.05$ from Kormendy & Bender (2013) and $\sigma_e = 222 \pm 11 \text{ km s}^{-1}$ from Davis et al. (2013), but we checked that σ_e is consistent with our definition of how to average $V^2(r) + \sigma^2(r)$. The asymptotic circular velocity is from Pellegrini, Held, & Ciotti (1997), but it is uncertain whether the measured rotation curve reaches far enough out in this and almost any bulge-dominated S0.

NGC 4594 = M104 = the Sombrero Galaxy: The BH discovery paper was Kormendy (1988), who obtained $M_\bullet = 5.5(1.7 - 17) \times 10^8 M_\odot$. The quoted error bar was conservative, but the best-fitting mass was within 17% of the present adopted value, $M_\bullet = 6.65(6.24 - 7.05) \times 10^8 M_\odot$ (Jardel et al. 2011). The BH detection was confirmed at HST resolution by Kormendy et al. (1996a), but the mass was estimated only by reobserving at HST resolution a set of models that were designed for ground-based data. As a result, $M_\bullet \sim 1.1 \times 10^9 M_\odot$ was not very accurate. Emsellem et al. (1994) measured $M_\bullet \sim 5.3 \times 10^8 M_\odot$ and Magorrian et al. (1998) got $M_\bullet = 6.9(6.7 - 7.0) \times 10^8 M_\odot$ based on two-integral models. The presently adopted BH mass is based on three-integral models.

We adopt the total magnitude measurement $B_T = 8.71$ in Burkhead (1986) and correct the 2MASS K magnitude to give $(V - K)_0 = 2.980$. Also, V_{circ} is from Faber et al. (1977) and Bajaja et al. (1984).

NGC 4596: We adopt the $M_{\text{BH,fix}}$ mass in Table 2 of Sarzi et al. (2001). Also, $B/T = 0.27 \pm 0.04$ comes from comparing Benedict’s (1976) decomposition at surface brightnesses $\lesssim 23.5 \text{ B mag arcsec}^{-2}$ with the adopted total magnitude $B_T = 11.37$, i.e., the mean of values in RC3, the Hyperleda main table, and the Hyperleda integrated photometry table. The rotation velocity corrected for asymmetric drift is from Kent (1990).

NGC 7457: We confirm Gültekin’s value of $\sigma_e = 67 \pm 3 \text{ km s}^{-1}$ with our photometry and kinematic measurements. The outer disk circular velocity is from our kinematic data and those of Cherepashchuk et al. 2010, corrected for asymmetric drift by them but for our assumed inclination of the galaxy, $i = 59^\circ \pm 2^\circ$.

S4.3. Notes on Individual Disk Galaxies with Pseudobulges

Our Galaxy: Photometric parameters are discussed in Kormendy & Bender (2013). Our Galaxy requires special procedures because we live inside it. For the convenience of readers, we summarize the provenance of the photometric parameters here. The Galaxy has a boxy bulge (e.g., Weiland et al. 1994; Dwek et al. 1995; Wegg & Gerhard 2013) that is understood as an almost-end-on bar (Combes & Sanders 1981; Blitz & Spergel 1991). It is therefore a pseudobulge – a component built out of the disk. There is no photometric or kinematic sign of a classical bulge (see Freeman 2008, Howard et al. 2009, Shen et al. 2010, and Kormendy et al. 2010 for reviews and for some of the evidence). We average pseudobulge-to-total luminosity ratios from Kent, Dame & Fazio (1991) and Dwek et al. (1995) to get $PB/T = 0.19 \pm 0.02$. To get $M_{K_{ST}} = -23.7$, we adopt the total K -band luminosity $L_K = 6.7 \times 10^{10} L_{K\odot}$ from Kent, Dame & Fazio (1991) and convert it from their assumed distance of 8 kpc to our assumed distance of 8.28 kpc from Genzel et al. (2010). The disk and pseudobulge absolute magnitudes follow from PB/T . Finally, V -band magnitudes are derived from K -band magnitudes by assuming that $(V - K)_0 = 2.980$. The bulge absolute magnitude is reasonably accurate, because the bulge is old; the main effect of estimating $M_{V,\text{bulge}}$ from $M_{K,\text{bulge}}$ is to implicitly correct for internal extinction. The disk magnitude is much more uncertain, because the assumed color does not take young stars into account. However, this has only minimal effects on our conclusions.

The adopted BH mass is now securely derived from the orbits of individual stars. The history of the remarkable improvement in M_\bullet measurements is reviewed in Genzel et al. (2010); early stages were covered in KR95. The velocity dispersion σ_e is from Gültekin et al. (2009c).

Circinus is like M31 in structure and inclination, but it is a smaller galaxy with a gas-rich pseudobulge, and it has a smaller BH than M31. It is a difficult case, because it is close to the Galactic plane. The Galactic absorption is large, and our estimates of it are uncertain. Kormendy & Bender (2013) measure the galaxy’s photometric parameters; the total apparent magnitude is $K_T = 4.71$. The pseudobulge classification and $PB/T = 0.30 \pm 0.03$ are from the same paper and from Fisher & Drory (2010). We adopt $V_T = 10.60 \pm 0.04$ as the average of values tabulated in the RC3 (de Vaucouleurs et al. 1991) and Hyperleda (Paturel et al. 2003). Comparing K_T and V_T in the context of various published estimates of the Galactic absorption, we adopt $A_V = 3.15$ from Karachentsev et al. (2004), because it gives the most reasonable total color for the galaxy, $(V - K)_0 = 3.05$. This then determines the other photometric parameters, including the distance $D = 2.82 \text{ Mpc}$ (Karachentsev et al. 2004).

Greenhill et al. (2003) measure masers both in outflowing gas and in a well-defined, essentially edge-on accretion disk. The latter masers show a well-defined Keplerian rotation curve which implies that $M_\bullet = (1.14 \pm 0.20) \times 10^6 M_\odot$. We adopt this value, although Huré et al. (2011) find hints that M_\bullet may be smaller. We are uncomfortable about the conflicting published velocity dispersion measurements: Oliva et al. (1995) measure 168 km s^{-1} consistently (RMS = 10 km s^{-1}) from four infrared CO bands; their instrumental resolutions ($\sigma_{\text{instr}} \simeq 80$ and 51 km s^{-1}) should be sufficient. But Maiolino et al. (1998) measure $\sigma \simeq 79 \pm 3 \text{ km s}^{-1}$ at $\sigma_{\text{instr}} \simeq 64 \text{ km s}^{-1}$ in the 2.3–2.4 μm CO bands using an integral-field spectrograph and AO; there is little gradient in the central $1''/2$ except that the nucleus has a bulge-subtracted velocity dispersion of $\sigma = 55 \pm 15 \text{ km s}^{-1}$. More recently, Mueller Sánchez et al. (2006) use SINFONI AO integral-field spectroscopy on the VLT to measure $\sigma \simeq 80 \text{ km s}^{-1}$ in the central $0''.4 \times 0''.4$. We adopt $\sigma_e = 79 \pm 3 \text{ km s}^{-1}$.

NGC 1068 is a prototypical oval galaxy (Kormendy & Kennicutt 2004) with an unusually massive pseudobulge that is more than a magnitude more luminous and a factor of ~ 4 more massive than the classical bulge of M31. Kormendy & Bender (2013) find that the pseudobulge-to-total luminosity ratio is quite different in the optical and infrared; $PB/T \simeq 0.41$ at H but $\simeq 0.3$ at r and i . We use these values at K and V , respectively. We adopt $\sigma_e = 151 \pm 7 \text{ km s}^{-1}$ from Gültekin et al. (2009c) and $V_{\text{circ}} = 283 \pm 9 \text{ km s}^{-1}$ from Hyperleda but note that the latter value is uncertain. We know of no two-dimensional analysis of the outer velocity field that takes the two differently oriented nested ovals into account; for a galaxy that is close to face-on, this is very important.

The BH discovery papers are Gallimore et al. (1996) and Greenhill et al. (1996) who found and measured positionally resolved H_2O maser emission with the VLA and with VLBA, respectively. The case is not as clean as that in NGC 4258, because the rotation velocity in the non-systemic-velocity sources decreases with increasing radius more slowly than a Keplerian, $V(r) \propto r^{-0.31 \pm 0.02}$ (Greenhill et al. 1996). The simplest and most plausible explanation is that the mass of the masing disk is not negligible with respect to the BH. Ignoring this, the above papers derive a first approximation to M_\bullet of $1 \times 10^7 M_\odot$. Greenhill & Gwinn (1997a) report additional VLBI observations and refine the total mass to

$1.54 \times 10^7 M_\odot$. Lodato & Bertin (2003) confirm this: they get $M_\bullet = (1.66 \pm 0.02) \times 10^7 M_\odot$ using the approximation of a Keplerian rotation curve. However, both Lodato & Bertin (2003) and Huré (2002; see also Huré et al. 2011) derive models that account for the disk mass, and we adopt the average of their results, $M_\bullet = (8.39 \pm 0.44) \times 10^6 M_\odot$ (Section 3.3.3).

Note again the extreme misalignment of the maser disk, which is essentially edge-on, and the rest of the galaxy, which is $\sim 21^\circ$ from face-on.

NGC 1300: We adopt D (Local Group) = 21.5 Mpc, consistent with the distances to neighbors NGC 1297 and NGC 1232, all members of grouping 51 –7 +4 (Tully 1988). However, Tonry et al. (2001) find $D = 28.5$ Mpc for NGC 1297. We cannot tell whether there is a problem with one of the distances or whether NGC 1297 is fortuitously close to NGC 1300 in the sky but behind it by half of the distance from us to the Virgo cluster. This is one example of a general problem: Distances remain uncertain, and we do not fold these uncertainties into our error estimates.

The effective radius of the pseudobulge is $r_e \simeq 4''.5 \pm 0''.1$ (Fisher & Drory 2008; Weinzirl et al. 2009). For σ_e , we use the mean dispersion 88 ± 3 km s⁻¹ interior to $3''.5$ as shown in Figure 6 of Batcheldor et al. (2005).

NGC 2273: We calculate $\sigma_e = 125 \pm 9$ km s⁻¹ from our photometry and from kinematic data in Barbosa et al. (2006).

NGC 2787 is an example of a phenomenon that must be moderately common – a galaxy that contains both a classical and a pseudo bulge. Erwin et al. (2003) make a decomposition with $B/T = 0.11$ and $PB/T = 0.26$. We adopt this decomposition to make the above point. However, at our present level of understanding, trying to separate bulges from pseudobulges is risky. In other galaxies, we identify the dominant component and assign all of the (pseudo)bulge light to it. Here, too, Columns 6 and 11 list the magnitudes of the bulge and pseudobulge together, and we treat this as a pseudobulge galaxy. The outer rotation velocity V_{circ} is from Shostak (1987) and from van Driel & van Woerden (1991).

NGC 3227: We use the corrected SBF $D = 23.75$ Mpc for companion galaxy NGC 3226 (Tonry et al. 2001). Mundell et al. (1995) provide V_{circ} .

NGC 3368 is a pseudobulge-dominated S(oval)ab spiral galaxy with a central decrease in σ at $r < 1''$ (Nowak et al. 2010). As emphasized by these authors, different definitions give different values of σ_e and this affects whether or not the BH falls within the scatter of the $M_\bullet - \sigma_e$ relation. Luminosity-weighted within the VLT SINFONI field of view of $3'' \times 3''$, $\sigma = 98.5$ km s⁻¹ and the BH is consistent with $M_\bullet - \sigma_e$. However, we use the definition that σ_e^2 is the luminosity-weighted mean of $V^2 + \sigma^2$ within approximately r_e (the exact radius makes little difference). Because rotation contributes and because $r_e \simeq 11''.2 \pm 2''.7$ for the pseudobulge, we get a substantially larger value of $\sigma_e \simeq 125 \pm 6$ km s⁻¹. This is based on our photometry and on kinematic data in Héraudeau et al. (1999) corrected inside $r_e/2$ to agree with Nowak et al. (2010). Sarzi et al. (2002) derived $\sigma_e = 114 \pm 8$ km s⁻¹ using dispersions only; this shows approximately how much difference rotation makes to the definition. Many pseudobulge galaxies are similar in that central velocity dispersions are much smaller than the σ_e that is obtained from the $V^2 + \sigma^2$ definition.

Nowak et al. (2010) suggest that NGC 3368 contains a small classical bulge in addition to the dominant pseudobulge. We add them together.

NGC 3384: Gültekin et al. (2009c) used $\sigma_e = 143 \pm 7$ km s⁻¹. We essentially confirm this: With our photometry and kinematic measurements, we get $\sigma_e = 150 \pm 8$ km s⁻¹. We adopt the mean.

NGC 3393 is another prototypical oval galaxy with a large pseudobulge. **Figure 10** is included to emphasize its similarity to NGC 1068: It is only $\sim 13^\circ$ from face-on (Cooke et al. 2000), but it contains an edge-on, masing accretion disk.

All measurements of this galaxy are somewhat uncertain. Kormendy & Bender (2013) find a preliminary $PB/T = 0.27 \pm 0.06$. The BH mass measurement is based on the rotation curve of a masing molecular disk (Kondratko, Greenhill & Moran 2008). The maser sources are well distributed along a line indicative of an edge-on disk, but they cover only a small radius range, so they do not securely measure the rotation curve shape. They are consistent with Keplerian; this gives an enclosed mass of $M_\bullet = (3.4 \pm 0.2) \times 10^7 M_\odot$ at $r \leq 0.40 \pm 0.02$ pc for our $D = 49.2$ Mpc. But there are signs that the rotation curve is slightly flatter than Keplerian. For their best-fitting sub-Keplerian rotation curve, Kondratko et al. (2008) get $M_\bullet \simeq 3 \times 10^7 M_\odot$. In contrast, Huré et al. (2011) find a good solution with a maser disk that is 6 times as massive as the BH. Then $M_\bullet \simeq 0.6 \times 10^7 M_\odot$. This is the only galaxy in our sample in which two such analyses give substantially different results. We adopt the mean of the two masses and half of the difference as our error estimate.

The velocity dispersion σ_e is securely measured by Greene et al. (2010), but V_{circ} is too uncertain, because the galaxy is too close to face-on.

NGC 3489 is a weakly barred S0 with a dominant (pseudo)bulge that contributes $\sim 35\%$ of the light of the galaxy (Nowak et al. 2010). These authors argue plausibly that about one-third of this component is a classical bulge. We conservatively add them together. Also, we derive $\sigma_e = 113 \pm 4$ km s⁻¹ from our photometry and kinematic data in McDermid et al. (2006).

NGC 4388: We have only central velocity dispersion data for this galaxy. Greene et al. (2010) measure $\sigma = 107 \pm 7$ km s⁻¹; Ho et al. (2009) get 91.7 ± 9.5 km s⁻¹, and we adopt the average, $\sigma_e = 99 \pm 10$ km s⁻¹. This is likely to be an underestimate of σ_e as we define it, because it neglects rotation inside the half-light radius $r_e \simeq 3''.0$ of the pseudobulge.

NGC 4736 and NGC 4826: We are most grateful to Karl Gebhardt for making M_\bullet available before publication (Gebhardt et al. 2013). For NGC 4736, we calculated σ_e from our photometry (Kormendy & Bender 2013) and kinematic data in Möllenhoff et al. (1995). For NGC 4826, σ_e is from our photometry and kinematic data in Rix et al. (1995). For both galaxies, the result is not significantly different if we integrate inside the pseudobulge $r_e \simeq 9''.7$ and $16''.7$, respectively (Fisher & Drory 2008) or inside $r_e/2$. Sources for V_{max} are given in Kormendy et al. (2010).

NGC 4945 is an edge-on, dusty Scd with a small pseudobulge ($PB/T = 0.07$) that is heavily absorbed at optical wavelengths. We use $D = 3.58$ Mpc, i. e., the mean of two TRGB distances determined from the magnitude of the tip of the red giant branch in the stellar color-magnitude diagram (3.36 Mpc: Mouhcine et al. 2005 and 3.80 Mpc: Mould & Sakai 2008). We adopt $K_T = 4.438$, i. e., the integral of the surface brightness and ellipticity profiles measured in Kormendy & Bender (2013). For comparison, 2MASS lists $K_s = 4.483$. Our total magnitude implies a slightly more plausible color $(V - K)_0 = 2.80$.

The BH detection in Greenhill, Moran & Herrnstein (1997b) was rejected by Gültekin et al. (2009c) because the maser rotation curve is asymmetric and because the maser disk inclination is only approximately constrained to be edge-on by its linear distribution at PA $\approx 45^\circ$. Still, because the disk is masing and masing requires a long line-of-sight path length, the assumption that the disk is edge-on is at least as secure as many other assumptions that we routinely make. And the rotation curve decreases cleanly with radius on one side of the center. Thus M_\bullet is not more uncertain than the most problematic cases based on stellar and ionized gas dynamics.

The maser disk and the galaxy disk have similar PA, are similarly edge-on, and rotate in the same direction (Greenhill et al. 1997b).

NGC 6264 and NGC 6323 are the most distant disk galaxies with maser BH detections. Kormendy & Bender (2013) measure r - and K -band brightness profiles, respectively. No HST imaging is available for either galaxy, although CFHT images with PSF dispersion radii of $\sigma_* = 0''.23$ are available for NGC 6323. Both galaxies have small pseudobulges; NGC 6264 has $PB/T \simeq 0.17 \pm 0.03$ and NGC 6323 has $PB/T \simeq 0.05 \pm 0.01$. For both galaxies, we adopt σ_e equal to the central velocity dispersion measured by Greene et al. (2010).

IC 2560: Evidence for a BH based on the dynamics of a H₂O maser disk was reported in Ishihara et al. (2001) and refined with further observations in Yamauchi et al. (2012). We adopt M_\bullet and its upper error bar from the latter paper. However, only one point in the rotation curve is observed from high- $|V|$ masers, so we cannot tell whether the rotation curve is Keplerian. Centripetal acceleration of the systemic masers is accurately measured, but their velocity gradient with position along the major axis of the disk is not accurately enough known to give a second meaningful $V(r)$ point as discussed in Section 3.3.2. Since some maser disks have gas masses that are significant fractions of the BH masses, we must regard the BH mass determination for IC 2560 as an upper limit. Nevertheless, M_\bullet is clearly small enough to support our conclusion that BHs do not correlate with pseudobulges in the same way as they do with classical bulges.

We have only a central velocity dispersion measurement (Greene et al. 2010). The outer rotation velocity V_{circ} is from Hyperleda.

UGC 3789: We adopt the geometric distance $D = 49.9 \pm 7.0$ Mpc from Braatz et al. (2010). It provides a check of our D (Local Group) distances (Table 3, Column 3, source 9); this distance would have been 47.8 Mpc. The K magnitude is from 2MASS, but the V magnitude is estimated from K using a photoelectric measurement of $B - V = 0.92$ in a $50''$ diameter aperture by Arhipova & Saveleva (1984). The correlation of $(V - K)_0$ with $(B - V)_0$ then gives $(V - K)_0 \simeq 2.90$.

UGC 3789 is another example of a common phenomenon for which we know no explanation: It is a prototypical, almost-face-on oval galaxy with an edge-on molecular disk surrounding the BH (Figure 10). The velocity dispersion is from Greene et al. (2010) and V_{circ} is from Hyperleda.

S4.4. Notes on Discarded Galaxies (Purple Lines in Tables 2 and 3):

NGC 2778 is discarded (1) because it provides only an upper limit on M_{\bullet} (Schulze & Gebhardt 2011) and (2) because the implied mass-to-light ratio $M/L_K = 3.3$ is too large for an old stellar population from which the dark matter has been subtracted and modeled separately (Section 6.6). We conclude that dark matter is still included and therefore that the M_{\bullet} upper limit is substantially too small. This galaxy is a good illustration of the importance of adding M/L constraints to our mass measurements, something that has not heretofore been done

NGC 3607 is a core elliptical with a BH detection and M_{\bullet} measurement in Gültekin et al. (2009b). The modeling did not include dark matter. Schulze & Gebhardt (2011) and Rusli et al. (2013) show that this is not a large problem if r_{infl} is very well resolved, but they show that M_{\bullet} is systematically underestimated if $r_{\text{infl}}/\sigma_* \lesssim 5$. Both papers provide calibrations of how the M_{\bullet} correction factor depends on r_{infl}/σ_* , but the two calibrations disagree even though they both use variants of the Nuker code. The disagreement may result from technical details such as the number of orbits used in the modeling. But the problem is severe for NGC 3607, for which the apparent value of $r_{\text{infl}}/\sigma_* \simeq 1.5$. Based on the Schulze calibration, we should multiply the Gültekin $M_{\bullet} = 1.4 \times 10^8 M_{\odot}$ (Figure 12) by a factor of ~ 2 . The Rusli calibration gives a factor of ~ 4.7 . We conclude that the BH detection is reliable but that we do not know the BH mass well enough to retain NGC 3607 in our sample.

NGC 4261, NGC 6251, NGC 7052, A1836 BCG, and A3565 BCG: All of these galaxies have valid BH detections based on optical emission-line kinematic observations in the papers listed in Column 13. However, the widths of the emission lines are comparable to the rotation velocities near the center, and these widths were not taken into account in estimating M_{\bullet} . As discussed in the BH discovery papers and in Section 3.2 here, it is not guaranteed that line widths imply a “contribution” to M_{\bullet} as they would for absorption-line velocity dispersions. But it is likely that they are not ignorable. In Section 6.2 (Figure 12), we compare these BH masses to the BH–host-galaxy correlations that we derive for the most reliable BH masses. We find that the above galaxies do indeed have anomalously small BH masses. The conservative conclusion therefore is that neglecting emission-line widths can result in underestimated BH masses. We therefore omit all such masses, even those for lower-luminosity bulges in which the measured M_{\bullet} does not obviously deviate from the correlations (e. g., NGC 4459).

Cygnus A: The BH discovery (Tadhunter et al. 2003) is based on the optical emission-line rotation curve measured with HST STIS. The authors note that the emission lines are very broad, but they do not include line widths in their M_{\bullet} determination. Therefore the BH mass is probably underestimated. The velocity dispersion is from Thornton et al. (1999) and is very uncertain; it is based on the observed width of the Ca infrared triplet absorption lines but not on any of the standard methods of comparing the spectrum to a standard star. Finally, although we used the brightest V -band magnitude in the literature (from Paturel et al. 2000 as listed by Hyperleda), the $(V - K)_0 = 3.54$ color is implausibly large. It may be affected by large internal absorption. If so, the K -band magnitude may be usable. Nevertheless, for all of the above reasons, this galaxy is plotted in Section 6.2 (Figure 12) and thereafter is omitted from all correlations and fits.

ACKNOWLEDGMENTS

We warmly thank Mary Kormendy for help in proofreading this paper and in checking its references.

We made extensive use of NASA’s Astrophysics Data System bibliographic services and the NASA/IPAC Extragalactic Database (NED). NED is operated by the Jet Propulsion Laboratory and the California Institute of Technology under contract with NASA. We also used the HyperLeda electronic database (Paturel et al. 2003) at <http://leda.univ-lyon1.fr>. And we made extensive use of the Two Micron All Sky Survey (2MASS; Skrutskie et al. 2006). 2MASS is a joint project of the University of Massachusetts and the Infrared Processing and Analysis Center/California Institute of Technology, funded by NASA and the NSF.

JK’s research was supported in part by NSF grant AST-0607490. Also, this multi-year research project would not have been possible without the long-term support provided to JK by the Curtis T. Vaughan, Jr. Centennial Chair in Astronomy. We are most sincerely grateful to Mr. and Mrs. Curtis T. Vaughan, Jr. for their continuing support of Texas astronomy. JK also warmly thanks Ralf Bender and the staffs of the University Observatory, Ludwig-Maximilians-University, Munich, Germany and the Max-Planck-Institute for Extraterrestrial Physics, Garching-by-Munich, Germany for their support and hospitality during several visits during which much of this review was written.

LCH’s work is supported by the Carnegie Institution for Science and by NASA grants from the Space Telescope Science Institute (operated by AURA, Inc., under NASA contract NAS5-26555). LCH thanks the Chinese Academy of Sciences and the hospitality of the National Astronomical Observatories, where part of this review was written.

SUPPLEMENTARY LITERATURE CITED

- Arhipova, V. P., & Saveleva, M. V. 1984, Trudy Gosudarstvennogo Astronomicheskogo Instituta P. K. Sternberga, 54, 33
 Atkinson, J. W., Collett, J. L., Marconi, A., et al. 2005, MNRAS, 359, 504
 Bahcall, J. N., Kozlovsky, B.-Z., & Salpeter, E. E. 1972, ApJ, 171, 467
 Bajaja, E., van der Burg, G., Faber, S. M., et al. 1984, A&A, 141, 309
 Barbosa, F. K. B., Storchi-Bergmann, T., Cid Fernandes, R., Winge, C., & Schmitt, H. 2006, MNRAS, 371, 170
 Barth, A. J., Pancoast, A., Thorman, S. J., et al. 2011, ApJ, 743, L4
 Barth, A. J., Sarzi, M., Rix, H.-W., et al. 2001, ApJ, 555, 685
 Baskin, A., & Laor, A. 2005, MNRAS, 356, 1029
 Batcheldor, D., Axon, D., Merritt, D., et al. 2005, ApJS, 160, 76
 Bender, R., Kormendy, J., Bower, G., et al. 2005, ApJ, 631, 280
 Benedict, G. F. 1976, AJ, 81, 799
 Bennert, N., Schulz, H., & Henkel, C. 2004, A&A, 419, 127
 Bentz, M. C., Peterson, B. M., Netzer, H., Pogge, R. W., & Vestergaard, M. 2009a, ApJ, 697, 160
 Bentz, M. C., Peterson, B. M., Pogge, R. W., Vestergaard, M., & Onken, C. A. 2006, ApJ, 644, 133
 Bentz, M. C., Walsh, J. L., Barth, A. J., et al. 2008, ApJ, 689, L21

- Bentz, M. C., Walsh, J. L., Barth, A. J., et al. 2009b, *ApJ*, 705, 199
- Bentz, M. C., Walsh, J. L., Barth, A. J., et al. 2010, *ApJ*, 716, 993
- Bessell, M. S. 2005, *ARA&A*, 43, 293
- Blakeslee, J. P., Cantiello, M., Mei, S., et al. 2010, *ApJ*, 724, 657
- Blakeslee, J. P., Jordán, A., Mei, S., et al. 2009, *ApJ*, 694, 556
- Blandford, R. D., & McKee, C. F. 1982, *ApJ*, 255, 419
- Blitz, L., & Spergel, D. N. 1991, *ApJ*, 379, 631
- Bochkarev, N. G., & Gaskell, C. M. 2009, *ALet*, 35, 287
- Bower, G. A., Green, R. F., Bender, R., et al. 2001, *ApJ*, 550, 75
- Bower, G. A., Green, R. F., Danks, A., et al. 1998, *ApJ*, 492, L111
- Bower, G. A., Heckman, T. M., Wilson, A. S., & Richstone, D. O. 1997, *ApJ*, 483, L33
- Bower, G. A., Wilson, A. S., Heckman, T. M., et al. 2000, *BAAS*, 32, 1566
- Braatz, J. A., Reid, M. J., Humphreys, E. M. L., et al. 2010, *ApJ*, 718, 657
- Brewer, B. J., Treu, T., Pancoast, A., et al. 2011, *ApJ*, 733, L33
- Burkhead, M. S. 1986, *AJ*, 91, 777
- Cappellari, M., Neumayer, N., Reunanen, J., et al. 2009, *MNRAS*, 394, 660
- Cappellari, M., Scott, N., Alatalo, K., et al. 2013, *MNRAS*, 432, 1709
- Cappellari, M., Verolme, E. K., van der Marel, R. P., et al. 2002, *ApJ*, 578, 787
- Carpenter, J. M. 2001, *AJ*, 121, 2851
- Chemin, L., Carignan, C., & Foster, T. 2009, *ApJ*, 705, 1395
- Cherepashchuk, A. M., Afanas'ev, V. L., Zasov, A. V., & Katkov, I. Yu. 2010, *Astr. Reports*, 54, 578
- Cherepashchuk, A. M., & Lyutyi, V. M. 1973, *ApLet*, 13, 165
- Collin, S., Kawaguchi, T., Peterson, B. M., & Vestergaard, M. 2006, *A&A*, 456, 75
- Combes, F., & Sanders, R. H. 1981, *A&A*, 96, 164
- Cooke, A. J., Baldwin, J. A., Ferland, G. J., Netzer, H., & Wilson, A. S. 2000, *ApJS*, 129, 517
- Courteau, S., Widrow, L. M., McDonald, M., et al. 2011, *ApJ*, 739, 20
- Cretton, N., & van den Bosch, F. C. 1999, *ApJ*, 514, 704
- Croom, S. M. 2011, *ApJ*, 736, 161
- Dalla Bontà, E., Ferrarese, L., Corsini, E. M., et al. 2009, *ApJ*, 690, 537
- Davies, R. I., Thomas, J., Genzel, R., et al. 2006, *ApJ*, 646, 754
- Davis, T. A., Bureau, M., Cappellari, M., Sarzi, M., & Blitz, L. 2013, *Nature*, 494, 328
- De Francesco, G., Capetti, A., & Marconi A. 2006, *A&A*, 460, 439
- De Francesco, G., Capetti, A., & Marconi A. 2008, *A&A*, 479, 355
- Denney, K. D. 2012, *ApJ*, 759, 44
- Denney, K. D., Peterson, B. M., Pogge, R. W., et al. 2009, *ApJ*, 704, L80
- Denney, K. D., Peterson, B. M., Pogge, R. W., et al. 2010, *ApJ*, 721, 715
- de Vaucouleurs, G. 1961, *ApJS*, 6, 213
- de Vaucouleurs, G., de Vaucouleurs, A., Corwin, H. G., et al. 1991, *Third Reference Catalogue of Bright Galaxies* (Berlin: Springer) (RC3)
- Devereux, N., Ford, H., Tsvetanov, Z., & Jacoby, G. 2003, *AJ*, 125, 1226
- Dibai, É. A. 1977, *Sov. Astron. Lett.*, 3, 1
- Dibai, É. A. 1984, *Sov. Astron.*, 28, 245
- Dressler, A., & Sandage, A. 1983, *ApJ*, 265, 664
- Drory, N., & Fisher, D. B. 2007, *ApJ*, 664, 640
- Dwek, E., Arendt, R. G., Hauser, M. G., et al. 1995, *ApJ*, 445, 716
- Emsellem, E., Cappellari, M., Krajnović, D., et al. 2007, *MNRAS*, 379, 401
- Emsellem, E., Cappellari, M., Peletier, R. F., et al. 2004, *MNRAS*, 352, 721
- Emsellem, E., Dejonghe, H., & Bacon, R. 1999, *MNRAS*, 303, 495
- Emsellem, E., Monnet, G., Bacon, R., & Nieto, J.-L. 1994, *A&A*, 285, 739
- Erwin, P., Vega Beltrán, J. C., Graham, A. W., & Beckman, J. E. 2003, *ApJ*, 597, 929
- Faber, S. M., Balick, B., Gallagher, J. S., & Knapp, G. R. 1977, *ApJ*, 214, 383
- Faber, S. M., & Jackson, R. E. 1976, *ApJ*, 204, 668
- Falcke, H., KÖrding, E., & Markoff, S. 2004, *A&A*, 414, 895
- Ferrarese, L., & Ford, H. C. 1999, *ApJ*, 515, 583
- Ferrarese, L., Ford, H. C., & Jaffe, W. 1996, *ApJ*, 470, 444
- Ferrarese, L., & Merritt, D. 2000, *ApJ*, 539, L9
- Ferrarese, L., Pogge, R. W., Peterson, B. M., et al. 2001, *ApJ*, 555, L79

- Fisher, D. 1997, *AJ*, 113, 950
- Fisher, D. B., & Drory, N. 2008, *AJ*, 136, 773
- Fisher, D. B., & Drory, N. 2010, *ApJ*, 716, 942
- Freeman, K. C. 2008, in *Formation and Evolution of Galaxy Disks*, ed. J. G. Funes & E. M. Corsini (San Francisco, CA: ASP), 3
- Gallimore, J. F., Baum, S. A., O’Dea, C. P., Brinks, E., & Pedlar, A. 1996, *ApJ*, 462, 740
- Gaskell, C. M. 1988, *ApJ*, 325, 114
- Gaskell, C. M. 2008, *Rev. Mex. A&A*, 32, 1
- Gaskell, C. M. 2009, *NewAR*, 53, 140
- Gaskell, C. M. 2010, in *ASP Conference Series, Vol. 427, Accretion and Ejection in AGNs: A Global View*, ed. L. Maraschi, G. Ghisellini, R. Della Ceca, & F. Tavecchio (San Francisco: ASP), 68
- Gaskell, C. M. 2011, *Baltic A*, 20, 392
- Gaskell, C. M., & Sparke L. S. 1986, *ApJ*, 305, 175
- Gebhardt, K., Adams, J., Richstone, D., et al. 2011, *ApJ*, 729, 119
- Gebhardt, K., Kormendy, J., Ho, L. C., et al. 2000a, *ApJ*, 543, L5
- Gebhardt, K., Lauer, T. R., Pinkney, J., et al. 2007, *ApJ*, 671, 1321
- Gebhardt, K., Richstone, D., Kormendy, J., et al. 2000b, *AJ*, 119, 1157
- Gebhardt, K., Richstone, D., Tremaine, S., et al. 2003, *ApJ*, 583, 92
- Gebhardt, K., & Thomas, J. 2009, *ApJ*, 700, 1690
- Gebhardt, K., et al. 2013, in preparation
- Genzel, R., Eisenhauer, F., & Gillessen, S. 2010, *Rev. Mod. Phys.*, 82, 3121
- Graham, A. W., Colless, M. M., Busarello, G., Zaggia, S., & Longo, G. 1998, *A&AS*, 133, 325
- Graham, A. W., Onken, C. A., Athanassoula, E., & Combes, F. 2011, *MNRAS*, 412, 2211
- Graham, A. W., & Scott, N. 2013, *ApJ*, 764, 151
- Greene, J. E., & Ho, L. C. 2005, *ApJ*, 630, 122
- Greene, J. E., & Ho, L. C. 2006, *ApJ*, 641, L21
- Greene, J. E., & Ho, L. C. 2009, *PASP*, 121, 1167
- Greene, J. E., Peng, C. Y., Kim, M., et al. 2010, *ApJ*, 721, 26
- Greenhill, L. J., Booth, R. S., Ellingsen, S. P., et al. 2003, *ApJ*, 590, 162
- Greenhill, L. J., & Gwinn, C. R. 1997a, *ApSS*, 248, 261
- Greenhill, L. J., Gwinn, C. R., Antonucci, R., & Barvainis, R. 1996, *ApJ*, 472, L21
- Greenhill, L. J., Moran, J. M., & Herrnstein, J. R. 1997b, *ApJ*, 481, L23
- Grier, C. J., Peterson, B. M., Horne, K., et al. 2013, *ApJ*, 764, 47
- Grier, C. J., Peterson, B. M., Pogge, R. W., et al. 2012, *ApJ*, 755, 60
- Gültekin, K., Cackett, E. M., Miller, J. M., et al. 2009a, *ApJ*, 706, 404
- Gültekin, K., Richstone, D. O., Gebhardt, K., et al. 2009b, *ApJ*, 695, 1577
- Gültekin, K., Richstone, D. O., Gebhardt, K., et al. 2009c, *ApJ*, 698, 198
- Gültekin, K., Richstone, D. O., Gebhardt, K., et al. 2011, *ApJ*, 741, 38
- Hardcastle, M. J., Evans, D. A., & Croston, J. H. 2009, *MNRAS*, 396, 1929
- Häring-Neumayer, N., Cappellari, M., Rix, H.-W., et al. 2006, *ApJ*, 643, 226
- Harms, R. J., Ford, H. C., Tsvetanov, Z. I., et al. 1994, *ApJ*, 435, L35
- Henkel, C., Braatz, J. A., Greenhill, L. J., & Wilson, A. S. 2002, *A&A*, 394, L23
- Héraudeau, Ph., Simien, F., Maubon, G., & Prugniel, Ph. 1999, *A&AS*, 136, 509
- Herrnstein, J. R., Moran, J. M., Greenhill, L. J., et al. 1999, *Nature*, 400, 539
- Ho, L. C. 2008, *ARA&A*, 46, 475
- Ho, L. C., Goldoni, P., Dong, X.-B., Greene, J. E., & Ponti, G. 2012, *ApJ*, 754, 11
- Ho, L. C., Greene, J. E., Filippenko, A. V., & Sargent, W. L. W. 2009, *ApJS*, 183, 1
- Hopkins, P. F., Cox, T. J., Dutta, S. N., et al. 2009, *ApJS*, 181, 135
- Houghton, R. C. W., Magorrian, J., Sarzi, M., et al. 2006, *MNRAS*, 367, 2
- Howard, C. D., Rich, R. M., Clarkson, W., et al. 2009, *ApJ*, 702, L153
- Huang, S., Ho, L. C., Peng, C. Y., Li, Z.-Y., & Barth, A. J. 2013, *ApJ*, 766, 47
- Huré, J.-M. 2002, *A&A*, 395, L21
- Huré, J.-M., Hersant, F., Surville, C., Nakai, N., & Jacq, T. 2011, *A&A*, 530, 145
- Ishihara, Y., Nakai, N., Iyomoto, N., et al. 2001, *PASJ*, 53, 215
- Jardel J. R., Gebhardt, K., Shen, J., et al. 2011, *ApJ*, 739, 21

- Jarrett, T. H., Chester, T., Cutri, R., Schneider, S. E., & Huchra, J. P. 2003, *AJ*, 125, 525
- Johnson, H. L. 1962, *ApJ*, 135, 69
- Karachentsev, I. D., Karachentseva, V. E., Huchtmeier, W. K., & Makarov, D. I. 2004, *AJ*, 127, 2031
- Kaspi, S., Brandt, W. N., Maoz, D., et al. 2007, *ApJ*, 659, 997
- Kaspi, S., Maoz, D., Netzer, H., et al. 2005, *ApJ*, 629, 61
- Kaspi, S., Smith, P. S., Netzer, H., et al. 2000, *ApJ*, 533, 631
- Kent, S. M. 1990, *AJ*, 100, 377
- Kent, S. M., Dame, T. M., & Fazio, G. 1991, *ApJ*, 378, 131
- Kollatschny, W., & Zetzl, M. 2011, *Nature*, 470, 366
- Komatsu, E., Dunkley, J., Nolta, M. R., et al. 2009, *ApJS*, 180, 330
- Kondratko, P. T., Greenhill, L. J., & Moran, J. M. 2008, *ApJ*, 678, 87
- Koratkar, A. P., & Gaskell, C. M. 1989, *ApJ*, 345, 637
- Körding, E. 2008, in *Proceedings of the VII Microquasar Workshop: Microquasars and Beyond*, Foca, Izmir, Turkey; published online at <http://pos.sissa.it/cgi-bin/reader/conf.cgi?confid=62>, 23
- Kormendy, J. 1988, *ApJ*, 335, 40
- Kormendy, J. 1992a, in *Testing the AGN Paradigm*, ed. S. S. Holt, S. G. Neff, & C. M. Urry (New York: AIP), 23
- Kormendy, J. 1992b, in *High Energy Neutrino Astrophysics*, ed. V. J. Stenger, J. G. Learned, S. Pakvasa, & X. Tata (Singapore: World Scientific), 196
- Kormendy, J. 1999, in *ASP Conference Series, Vol. 182, Galaxy Dynamics: A Rutgers Symposium*, ed. D. Merritt, J. A. Sellwood, & M. Valluri (San Francisco: ASP), 124
- Kormendy, J., & Bender, R. 2012, *ApJS*, 198, 2
- Kormendy, J., & Bender, R. 2013, *Disk Galaxy Hosts of Dynamically Detected Supermassive Black Holes*, in preparation
- Kormendy, J., Bender, R., Ajhar, E. A., et al. 1996a, *ApJ*, 473, L91
- Kormendy, J., Bender, R., Evans, A. S., & Richstone, D. 1998, *AJ*, 115, 1823
- Kormendy, J., Bender, R., Magorrian, J., et al. 1997, *ApJ*, 482, L139
- Kormendy, J., Bender, R., Richstone, D., et al. 1996b, *ApJ*, 459, L57
- Kormendy, J., Drory, N., Bender, R., & Cornell, M. E. 2010, *ApJ*, 723, 54
- Kormendy, J., Fisher, D. B., Cornell, M. E., & Bender, R. 2009, *ApJS*, 182, 216 (KFCB)
- Kormendy, J., & Freeman, K. C., 2013, *Scaling Laws for Dark Matter Halos in Late-Type and Dwarf Spheroidal Galaxies*, in preparation
- Kormendy, J., Gebhardt, K., Fisher, D. B., et al. 2005, *AJ*, 129, 2636
- Kormendy, J., & Kennicutt, R. C. 2004, *ARA&A*, 42, 603
- Kormendy, J., & Richstone, D. 1992, *ApJ*, 393, 559
- Krajinović, D., McDermid, R. M., Cappellari, M., & Davies, R. L. 2009, *MNRAS*, 399, 1839
- Krajinović, D., Sharp, R., & Thatte, N. 2007, *MNRAS*, 374, 385
- Krolik, J. H. 2001, *ApJ*, 551, 72
- Kuo, C. Y., Braatz, J. A., Condon, J. J., et al. 2011, *ApJ*, 727, 20
- Lauer, T. R., Ajhar, E. A., Byun, Y.-I., et al. 1995, *AJ*, 110, 2622
- Lauer, T. R., Faber, S. M., Gebhardt, K., et al. 2005, *AJ*, 129, 2138
- Lauer, T. R., Faber, S. M., Lynds, C. R., et al. 1992, *AJ*, 103, 703
- Lauer, T. R., Gebhardt, K., Faber, S. M., et al. 2007, *ApJ*, 664, 226
- Lauer, T. R., Gebhardt, K., Richstone, D., et al. 2002, *AJ*, 124, 1975
- Lodato, G., & Bertin, G. 2003, *A&A*, 398, 517
- Lyuityi, V. M., & Cherepashchuk, A. M. 1972, *Astron. Tsirk.*, 688, 1
- Macchetto, F., Marconi, A., Axon, D. J., et al. 1997, *ApJ*, 489, 579
- Maciejewski, W., & Binney, J. 2001, *MNRAS*, 323, 831
- Magorrian, J., Tremaine, S., Richstone, D., et al. 1998, *AJ*, 115, 2285
- Maiolino, R., Krabbe, A., Thatte, N., & Genzel, R. 1998, *ApJ*, 493, 650
- Mamyoda, K., Nakai, N., Yamauchi, A., Diamond, P., & Huré, J.-M. 2009, *PASJ*, 61, 1143
- Marconi, A., Capetti, A., Axon, D. J., et al. 2001, *ApJ*, 549, 915
- Marconi, A., Pastorini, G., Pacini, F., et al. 2006, *A&A*, 448, 921
- Marziani, P., & Sulentic, J. W. 2012, *NewAR*, 56, 49
- McConnell, N. J., & Ma, C.-P. 2013, *ApJ*, 764, 184

- McConnell, N. J., Ma, C.-P., Gebhardt, K., et al. 2011a, *Nature*, 480, 215
- McConnell, N. J., Ma, C.-P., Graham, J. R., et al. 2011b, *ApJ*, 728, 100
- McConnell, N. J., Ma, C.-P., Murphy, J. D., et al. 2012, *ApJ*, 756, 179
- McDermid, R. M., Emsellem, E., Shapiro, K. L. et al. 2006, *MNRAS*, 373, 906
- McGill, K. L., Woo, J.-H., Treu, T., & Malkan, M. A. 2008, *ApJ*, 673, 703
- McLure, R. J., & Dunlop, J. S. 2004, *MNRAS*, 352, 1390
- McLure, R. J., & Jarvis, M. J. 2002, *MNRAS*, 337, 109
- Mei, S., Blakeslee, J. P., Côté, P., et al. 2007, *ApJ*, 655, 144
- Méndez-Abreu, J., Aguerri, J. A. L., Corsini, E. M., & Simonneau, E. 2008, *A&A*, 478, 353
- Merloni, A., Heinz, S., & Di Matteo, T. 2003, *MNRAS*, 345, 1057
- Miyoshi, M., Moran, J., Herrnstein, J., et al. 1995, *Nature*, 373, 127
- Möllenhoff, C., Matthias, M., & Gerhard, O. E. 1995, *A&A*, 301, 359
- Monachesi, A., Trager, S. C., Lauer, T. R., et al. 2011, *ApJ*, 727, 55
- Mouhcine, M., Ferguson, H. C., Rich, R. M., Brown, T. M., & Smith, T. E. 2005, *ApJ*, 633, 810
- Mould, J., & Sakai, S. 2008, *ApJ*, 686, L75
- Mueller Sánchez, F., Davies, R. I., Eisenhauer, F., et al. 2006, *A&A*, 454, 481
- Mundell, C. G., Pedlar, A., Axon, D. J., Meaburn, J., & Unger, S. W. 1995, *MNRAS*, 277, 641
- Nagino, R., & Matsushita, K. 2009, *A&A*, 501, 157
- Nelson, C. H., Green, R. F., Bower, G., Gebhardt, K., & Weistrop, D. 2004, *ApJ*, 615, 652
- Netzer, H. 1990, in *Active Galactic Nuclei*, ed. R. D. Blandford, H. Netzer, & L. Woltjer (Berlin: Springer), 57
- Netzer, H., Lira, P., Trakhtenbrot, B., Shemmer, O., & Cury, I. 2007, *ApJ*, 671, 1256
- Netzer, H., Maoz, D., Laor, A., et al. 1990, *ApJ*, 353, 108
- Netzer, H., & Marziani, P. 2010, *ApJ*, 724, 318
- Neumayer, N., Cappellari, M., Reunanen, J., et al. 2007, *ApJ*, 671, 1329
- Nowak, N., Saglia, R. P., Thomas, J., et al. 2007, *MNRAS*, 379, 909
- Nowak, N., Saglia, R. P., Thomas, J., et al. 2008, *MNRAS*, 391, 1629
- Nowak, N., Thomas, J., Erwin, P., et al. 2010, *MNRAS*, 403, 646
- Oliva, E., Origlia, L., Kotilainen, J. K., & Moorwood, A. F. M. 1995, *A&A*, 301, 55
- Onken, C. A., Ferrarese, L., Merritt, D., et al. 2004, *ApJ*, 615, 645
- Osterbrock, D. E., & Mathews, W. G. 1986, *ARA&A*, 24, 171
- Pancoast, A., Brewer, B. J., & Treu, T. 2011, *ApJ*, 730, 139
- Pancoast, A., Brewer, B. J., Treu, T., et al. 2012, *ApJ*, 754, 49
- Park, D., Woo, J.-H., Treu, T., et al. 2012, *ApJ*, 747, 30
- Paturel, G., Fang, Y., Petit, C., Garnier, R., & Rousseau, J. 2000, *A&AS*, 146, 19
- Paturel, G., Petit, C., Prugniel, Ph., et al. 2003, *A&A*, 412, 45
- Pellegrini, S., Held, E. V., & Ciotti, L. 1997, *MNRAS*, 288, 1
- Peterson, B. M. 2011, in *Narrow-Line Seyfert 1 Galaxies and Their Place in the Universe*, ed. L. Foschini, et al., <http://pos.sissa.it/cgi-bin/reader/conf.cgi?confid=126>, id. 32
- Peterson, B. M., Ferrarese, L., Gilbert, K. M., et al. 2004, *ApJ*, 613, 682
- Pinkney, J., Gebhardt, K., Bender, R., et al. 2003, *ApJ*, 596, 903
- Rix, H.-W., Kennicutt, R. C., Braun, R., & Waltherbos, R. A. M. 1995, *ApJ*, 438, 155
- Rusli, S. P. 2012, PhD Thesis, Ludwig-Maximilians-University, Munich, Germany; <http://edoc.ub.uni-muenchen.de/14493>
- Rusli, S. P., Thomas, J., Erwin, P., et al. 2011, *MNRAS*, 410, 1223
- Rusli, S. P., Thomas, J., Saglia, R. P., et al. 2013, *AJ*, 146, 45
- Saglia, R. P., Fabricius, M., Bender, R., et al. 2010, *A&A*, 509, A61
- Samurović, S., & Danziger, I. J. 2005, *MNRAS*, 363, 769
- Sánchez-Portal, M., Díaz, A. I., Terlevich, E., & Terlevich, R. 2004, *MNRAS*, 350, 1087
- Sandage, A. 1961, *The Hubble Atlas of Galaxies* (Washington, DC: Carnegie Institution of Washington)
- Sandage, A., & Bedke, J. 1994, *The Carnegie Atlas of Galaxies* (Washington, DC: Carnegie Institution of Washington)
- Sandage, A., & Tammann, G. A. 1981, *A Revised Shapley-Ames Catalog of Bright Galaxies* (Washington, DC: Carnegie Institution of Washington)
- Sarzi, M., Rix, H.-W., Shields, J. C., et al. 2001, *ApJ*, 550, 65
- Sarzi, M., Rix, H.-W., Shields, J. C., et al. 2002, *ApJ*, 567, 237

- Schlaflly, E. F., & Finkbeiner, D. P. 2011, *ApJ*, 737, 103
- Schlegel, D. J., Finkbeiner, D. P., & Davis, M. 1998, *ApJ*, 500, 525
- Schmidt, M., & Green, R. F. 1983, *ApJ*, 269, 352
- Schombert, J. 2011, arXiv:1107.1728
- Schulze, A., & Gebhardt, K. 2011, *ApJ*, 729, 21
- Scorza, C., & Bender, R. 1995, *A&A*, 293, 20
- Seigar, M. S., Barth, A. J., & Bullock, J. S. 2008, *MNRAS*, 389, 1911
- Sérsic, J. L. 1968, *Atlas de Galaxias Australes* (Córdoba: Obs. Astron. Univ. Nacional de Córdoba)
- Shen, J., & Gebhardt, K. 2010, *ApJ*, 711, 484
- Shen, J., Rich, R. M., Kormendy, J., et al. 2010, *ApJ*, 720, L72
- Shen, Y. 2013, *Bull. Astron. Soc. India*, 41, 61 (arXiv:1302.2643)
- Shen, Y., Greene, J. E., Strauss, M. A., Richards, G. T., & Schneider, D. P. 2008, *ApJ*, 680, 169
- Shen, Y., & Liu, X. 2012, *ApJ*, 753, 125
- Shen, Y., Richards, G. T., Strauss, M. A., et al. 2011, *ApJS*, 194, 45
- Shostak, G. S. 1987, *A&A*, 175, 4
- Silge, J. D., Gebhardt, K., Bergmann, M., & Richstone, D. 2005, *AJ*, 130, 406
- Simien, F., & Prugniel, Ph. 2000, *A&AS*, 145, 263
- Simien, F., & Prugniel, Ph. 2002, *A&A*, 384, 371
- Skrutskie, M. F., Cutri, R. M., Stiening, R., et al. 2006, *AJ*, 131, 1163
- Tadhunter, C., Marconi, A., Axon, D., et al. 2003, *MNRAS*, 342, 861
- Tempel, E., Tamm, A., & Tenjes, P. 2010, *A&A*, 509, A91
- Thomsen, B., Baum, W. A., Hammergren, M., & Worthey, G. 1997, *ApJ*, 483, L37
- Thornton, R. J., Stockton, A., & Ridgway, S. E. 1999, *AJ*, 118, 1461
- Tonry, J. L., Dressler, A., Blakeslee, J. P., et al. 2001, *ApJ*, 546, 681
- Tremaine, S., Gebhardt, K., Bender, R., et al. 2002, *ApJ*, 574, 740
- Trevese, D., Paris, D., Stirpe, G. M., Vagnetti, F., & Zitelli, V. 2007, *A&A*, 470, 491
- Tully, R. B. 1988, *Nearby Galaxies Catalog* (Cambridge: Cambridge University Press)
- van den Bosch, R. C. E., & de Zeeuw, P. T. 2010, *MNRAS*, 401, 1770
- van den Bosch, R. C. E., Gebhardt, K., Gültekin, K., et al. 2012, *Nature*, 491, 729
- van der Marel, R. P. 1994a, *MNRAS*, 270, 271
- van der Marel, R. P. 1994b, *ApJ*, 432, L91
- van der Marel, R. P., & van den Bosch, F. C. 1998, *AJ*, 116, 2220
- van Driel, W., & van Woerden, H. 1991, *A&A*, 243, 71
- Verdoes Kleijn, G. A., van der Marel, R. P., Carollo, C. M., & de Zeeuw, P. T. 2000, *AJ*, 120, 1221
- Vestergaard, M. 2002, *ApJ*, 571, 733
- Vestergaard, M., & Peterson, B. M. 2006, *ApJ*, 641, 689
- Walsh, J. L., Barth, A. J., & Sarzi, M. 2010, *ApJ*, 721, 762
- Walsh, J. L., van den Bosch, R. C. E., Barth, A. J., & Sarzi, M. 2012, *ApJ*, 753, 79
- Walterbos, R. A. M., & Kennicutt, R. C. 1987, *A&AS*, 69, 311
- Wandel, A., & Yahil, A. 1985, *ApJ*, 295, L1
- Wang, J.-G., Dong, X.-B., Wang, T.-G., et al. 2009, *ApJ*, 707, 1334
- Wegg, C., & Gerhard, O. 2013, *MNRAS*, in press (arXiv:1308.0593)
- Weiland, J. L., Arendt, R. G., Berriman, G. B., et al. 1994, *ApJ*, 425, L81
- Weinzirl, T., Jogee, S., Khochfar, S., Burkert, A., & Kormendy, J. 2009, *ApJ*, 696, 411
- Wold, M., Lacy, M., Käuff, H. U., & Siebenmorgen, R. 2006, *A&A*, 460, 449
- Woo, J.-H. 2008, *AJ*, 135, 1849
- Woo, J.-H., Treu, T., Barth, A. J., et al. 2010, *ApJ*, 716, 269
- Xiao, T., Barth, A. J., Greene, J. E., et al. 2011, *ApJ*, 739, 28
- Yamauchi, A., Nakai, N., Ishihara, Y., Diamond, P., & Sato, N. 2012, *PASJ*, 64, 103
- Yuan, F., Yu, Z., & Ho, L. C. 2009, *ApJ*, 703, 1034